Applied Mathematical Modelling 40 (2016) 8530–8551

Contents lists available at ScienceDirect

Applied Mathematical Modelling

journal homepage: www.elsevier.com/locate/apm

A reduced-order model of mould heat transfer in the continuous casting of steel

Lance C. Hibbeler[a], Melody M. Chin See[b], Junya Iwasaki[c], Kenneth E. Swartz[a], Ronald J. O'Malley[d], Brian G. Thomas[a,*]

[a] The University of Illinois at Urbana-Champaign, Department of Mechanical Science and Engineering, Urbana, IL, United States
[b] Aerojet Rocketdyne, Flight Support Engineering, Systems Analysis and Software, United States
[c] Nippon Steel and Sumitomo Metal Corporation, Japan
[d] Missouri University of Science and Technology, Department of Materials Science and Engineering, United States

ARTICLE INFO

Article history:
Received 24 July 2015
Revised 23 March 2016
Accepted 13 April 2016
Available online 24 May 2016

Keywords:
Reduced-order model
Continuous casting
Mould heat transfer
Process modelling

ABSTRACT

A reduced-order model (ROM) of mould heat transfer in the continuous casting of steel is presented and demonstrated for several commercial mould geometries. The ROM relies on a physically-based solution of the one-dimensional heat-conduction equation. The up-front cost of the ROM is a single three-dimensional finite-element calculation of a small representative portion of the exact mould geometry, which is used to calibrate the geometric parameters of the ROM. Specifically, the ROM exactly matches the average hot and cold surface temperatures of the mould as computed in the snapshot model. Other features of the ROM, namely predictions of the cooling water temperature change and thermocouple temperatures, are derived in a manner consistent with the one-dimensional solution. Combined with models of solidification and mould-metal interfacial phenomena, this accurate and efficient modelling tool can be applied to enable deeper insight into many different aspects of heat transfer and related phenomena in the continuous casting process.

1. Introduction

"Reduced-order modelling" is a technique that seeks to reduce the complexity of a mathematical system while capturing the most significant behaviours and robustly maintaining the relationship between inputs and outputs. After an up-front cost to develop it, a reduced-order model (ROM) executes in a small fraction of the time of a full-order model with nearly the same accuracy. This reduction of complexity occurs by simplifying physical relationships, like linearising or decoupling physical phenomena, or by removing redundant or unimportant degrees of freedom. Least-squares regression is the simplest form of model reduction: a large number of points are replaced by a few polynomial coefficients that define a continuum relationship between variables. Reduced-order modelling techniques have been used for approximating: the transfer function in the solution of ordinary differential equations [1]; circuit analysis and design [2]; solid mechanics computations for structural dynamics [3,4], multi-body dynamics [5,6], and graphics rendering [7]; fluid-mechanics computations in a T-junction [8] and a backward-facing step [9–11]; fluid-structure interaction in MEMS devices [12] and aerospace applications [13–15]; and many other applications that need fast(er) calculation of important aspects of system behaviour.

* Corresponding author. Tel.: +1 2173336919.
E-mail address: bgthomas@illinois.edu (B.G. Thomas).

http://dx.doi.org/10.1016/j.apm.2016.04.002
0307-904X/

Nomenclature

Variables

A	Area
a_1, a_2	Coefficients in empirical equation
c_p	Isobaric specific heat capacity
D	Diameter
d	Depth or thickness
h	Heat transfer coefficient
k	Thermal conductivity of coating layer
ℓ	Length
n	Outward-pointing unit normal vector of surface
Nu	Nusselt number
Pe	Péclet number
Pr	Prandtl number
p	Pitch or pressure
Q	Volumetric flow rate
q	Heat flux
Re	Reynolds number
T	Temperature
V	Volume
v	Velocity
w	Width
x	Position vector $\{x, y, z\}$
α	Thermal diffusivity
β	Eigenvalue of fin temperature solution
μ	Dynamic shear viscosity
ρ	Mass density
θ	Scaled temperature

Subscripts

actual	Actual mould geometry
amb	Ambient medium for thermocouple
avg	Average
base	Base of fins
boil	Boiling
c	Cooling water channel
coat	Coating layer
cold	Cold face
foul	Fouling layer
gap	Mould/thermocouple gap
max	Maximum
meniscus	Meniscus
min	Minimum
mould	Mould
fins	Cooling fins
1D	One-dimensional (1D) model
plate	Mould plate, not including cooling fins
roots	Roots of water channels
strand	Strand
TC	Thermocouple
3D	Three-dimensional (3D) model
water	Cooling water
wire	Thermocouple wire

Adornments

$\bar{\phi}$	Average value
$\hat{\phi}$	Used to denote lateral surface area
ϕ^*	Scaled variable

ϕ'	Used to denote adjusted temperature
$\phi^{\diamond}$	Value used in model calibration

Reducing the degrees of freedom in a partial differential equation discretisation is the subject of recent literature, particularly in fluid mechanics. Proper-orthogonal decomposition [3,4,8,9,12–14,16], various modal-reduction techniques [5,6,10,11], or other reduced-basis methods [17] provide a reduced model that carries most of the character of a higher-order solution. Indeed, "reduced-basis" is a more specific description of these techniques, rather than the more general "reduced-order" that often is used in the literature. Reference [18] reviews the different reduced-basis approaches. These reduced-basis models are limited because the basis contains only information from the input "snapshot" model conditions, and the models lose accuracy when applied to significantly different conditions.

This work develops a reduced-order model of mould heat transfer in the continuous casting of steel. In the continuous casting process, molten metal flows under gravity from a ladle into a bottomless, water-cooled copper mould, where the metal begins to solidify. The solidifying "strand" is withdrawn from the bottom of the mould at a rate called the "casting speed," which matches the rate at which new metal solidifies. The mould region is shown in Fig. 1. Below the mould, the strand is sprayed with water to finish the solidification of the steel. Variants of this basic process are used to cast alloys of aluminium, copper, and magnesium.

A typical continuous slab-casting mould is shown in Figs. 1 and 2. The mould is assembled from four single-piece slabs of a copper alloy, *e.g.*, CuAg, CuBe, or CuCrZr, with cooling channels machined into the back side of each slab, shown in Fig. 2. Pressurised water flows through these channels at about 8 m/s to remove more than 1 MW of power from the solidifying metal. The total energy removed from the solidifying metal by the mould is tracked indirectly by measuring the temperature change of the cooling water. Some moulds include a thin coating layer of chromium, nickel, or a cermet to reduce the wearing of the "hot face," *i.e.*, the face of the mould in contact with the strand. Several bolt holes are machined into the back side of the mould, or the "cold face," for mounting the mould into its support structure and water-delivery system, collectively called the "waterbox." Moulds are instrumented with thermocouples, either between the water channels or coaxially with the bolt holes, for online monitoring of the casting process. The cooling water temperature change and mould thermocouple temperatures are the key validation and/or calibration points for models of mould heat transfer.

Modelling heat transfer in the continuous casting process requires accurate incorporation of the mould, the solidifying strand, and the interface between them. The interfacial heat transfer depends on the size of the gap, which is controlled by the shrinkage of the solidifying strand, which is coupled with the turbulent flow in the molten metal pool. The behaviour of the material in the gap, a ceramic slag, governs the heat extraction from the strand [19–21]. The cast product quality is governed by many coupled and nonlinear phenomena, which require advanced modelling techniques to gain the fundamental understanding needed to improve the process. The most important process phenomena are dependent upon the mould heat transfer, such as the rate-dependent solidification shrinkage of the solid shell, the rate-dependent flow and crystallisation or vitrification of the interfacial slag, and the multiphase turbulent flow of the molten metal with a free surface and particle

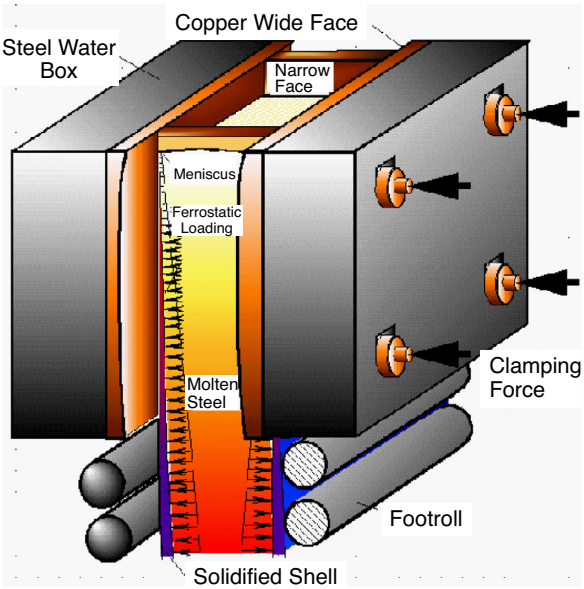

Fig. 1. Schematic of an assembled steel continuous casting mould.

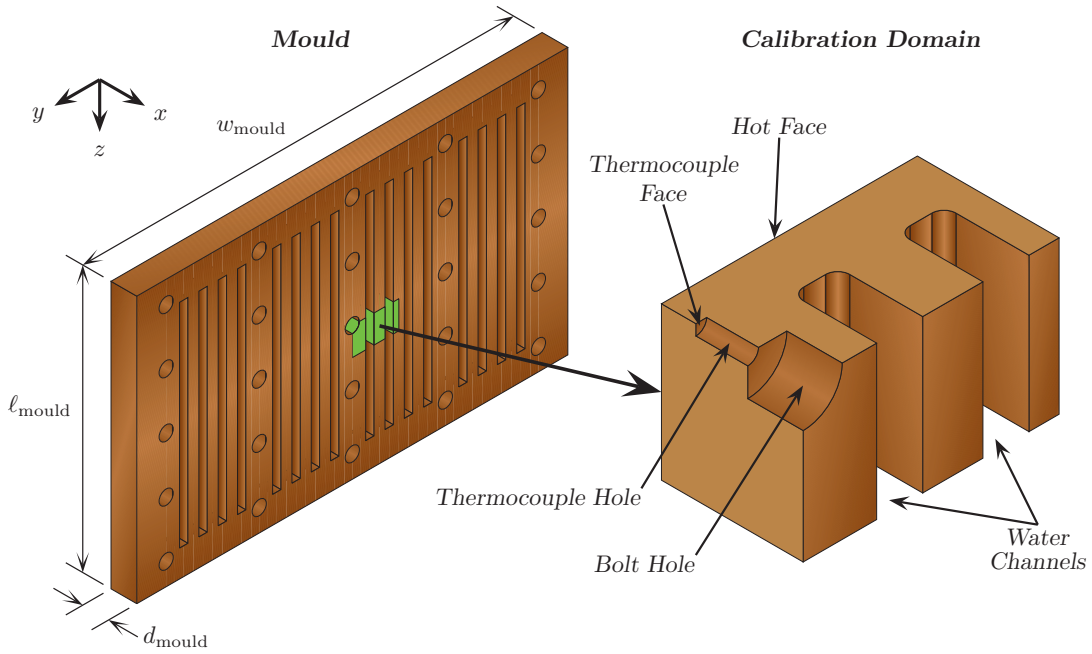

Fig. 2. Back of a typical continuous casting mould showing the calibration domain.

transport. Much of the previous work on these topics suffers from poor assumptions about mould heat transfer because modelling these complicated phenomena is so challenging; an often-used approach is trial-and-error calibration of an effective heat transfer coefficient (HTC). This work shows that, without much extra effort, the thermal behaviour of the mould can be modelled accurately.

The continuous casting literature has several examples of mould heat transfer models in one, two, and three dimensions with various levels of geometric complexity. Accurate computation of heat transfer in complicated-shaped moulds [22–25] and water channels [26–31] can be achieved only with models of high geometric complexity. Some mould heat transfer models investigate only phenomena related to mould heat transfer itself [19,25,28–36], and others use the calculated thermal behaviour to drive the expansion of the mould in investigations of mould distortion in billet [37–41], slab [42–44], funnel [26,45,46], and beam-blank [22] moulds. Models with simplified mould geometry have been used in inverse calculations of the heat extraction from the strand in billet [47–52] and slab [53–55] moulds.

Continuous casting process models have become more complicated in recent years by including multiple coupled phenomena. A few models solve for the temperatures and velocities in the cooling water [28,31,34], while all others use a heat transfer coefficient from an empirical correlation to model the thermal effect of the cooling water. Some models of the solidification shrinkage of the strand [22,56,57] and of the turbulent flow of the molten steel [53,58–60] include detailed models of mould heat transfer. The most complicated studies combined models of fluid flow, strand solidification and deformation, mould heat transfer, and mould distortion [23,24,61–63]; these studies all mention the difficulties of converging these coupled, multidomain, and multifield models. Though the mould heat transfer itself is a relatively easier problem, interfacing and iterating the mould simulations with models of other continuous casting phenomena quickly becomes computationally challenging. A simple-but-accurate model of mould heat transfer is needed for these complicated process models, but a reduced-order model of mould heat transfer is not found in the literature.

The reduced-order model of mould heat transfer presented in this work is part of the process model CON1D [19,64], which is a one-dimensional (1D) finite-difference model of the solidifying strand and includes simple models of solidification microscale physics, and lubrication and heat transfer in the strand-mould interface. The CON1D model has analysed several continuous casting machines [36,65,66], and its mould model has evolved from a 1D heat-conduction model with *ad hoc* corrections into the ROM presented in this work.

For the reduced-order model presented in this work, the dominant mode of heat transfer is determined *a priori* with scaling analysis [67], which motivates the closed-form 1D solution for the temperature in the mould that is presented in Section 2. The accuracy of the 1D temperature solution is improved by calibrating its geometric parameters with some of the geometry of the physical mould and with the calculated temperatures from a small three-dimensional (3D) finite-element model of a "unit cell" of the physical mould, which is discussed in Section 3. The calibration of the ROM is explained in Section 4, example calibrations are presented in Section 5, and the sensitivity of the ROM calibration is explored in Section 6. Section 7 shows some example applications of the ROM that is developed in this work.

2. Reduced-order model of mould heat transfer

The reduced-order model (ROM) developed in this work is based on the physics of the solution of the 1D heat-conduction equation, which is presented in Section 2.1, to provide a robust relationship between the boundary conditions and the mould temperatures. The governing equations and boundary conditions are presented more thoroughly in Section 3, and all symbols are summarised in the nomenclature section.

2.1. One-dimensional heat conduction analysis

The scaled [67] steady heat-conduction equation is

$$0 = \frac{\partial^2 \theta_{\text{mould}}}{\partial x^{*2}} + \left(\frac{d_{\text{mould}}}{w_{\text{mould}}}\right)^2 \frac{\partial^2 \theta_{\text{mould}}}{\partial y^{*2}} + \left(\frac{d_{\text{mould}}}{\ell_{\text{mould}}}\right)^2 \frac{\partial^2 \theta_{\text{mould}}}{\partial z^{*2}}, \tag{1}$$

where $\theta_{\text{mould}} = \left(T_{\text{mould}} - \bar{T}_{\text{water}}\right)/\left(T_{\text{mould,max}} - \bar{T}_{\text{water}}\right)$ is the mould temperature T_{mould} scaled by the maximum mould temperature $T_{\text{mould, max}}$ and cooling water bulk temperature $\bar{T}_{\text{water}}$, and $x^* = x/d_{\text{mould}}$, $y^* = y/w_{\text{mould}}$, and $z^* = z/\ell_{\text{mould}}$ are the coordinates scaled by the mould thickness d_{mould}, width w_{mould}, and length ℓ_{mould}. As illustrated in Fig. 2, the aspect-ratio terms in Eq. (1) are small, *i.e.*, $d_{\text{mould}}/w_{\text{mould}} \ll 1$ and $d_{\text{mould}}/\ell_{\text{mould}} \ll 1$, so the terms in which they appear can be neglected. This scaling analysis indicates that conduction through the thickness of the mould, *i.e.*, in the x-direction, is the dominant mode of heat transfer, and justifies the 1D assumption used to approximate the mould heat transfer.

The mould in the reduced-order model is envisioned as a rectangular plate with thickness d_{plate} and thermal conductivity k_{mould}, with a large number of identical rectangular fins welded to the "cold face" of the mould plate, which create water channels with depth d_c, width w_c, and pitch p_c, as shown in Fig. 3. The possible coating layer has thickness d_{coat} and thermal conductivity k_{coat}. The cold face of the mould is modelled as a convection condition with heat transfer coefficient h_{cold} and sink temperature $\bar{T}_{\text{water}}$, which are described in Sections 2.2 and 2.3. This treatment of the water channels allows the mould to be analysed as a number of thermal resistances, as shown in Fig. 4: heat is conducted through the mould plate into either the fins or the channel roots, and then into the cooling water.

The temperature in the mould $T_{1D}(x)$ is found by solving the 1D steady heat-conduction equation, which with constant thermal conductivity gives uniform heat flux throughout the mould. The solidifying steel supplies a heat flux $q_{\text{hot}} > 0$ to the hot face of the mould at $x = 0$, the temperature and heat flux are continuous across the coating-mould interface at $x = d_{\text{coat}}$, and the cold face at $x = d_{\text{coat}} + d_{\text{plate}}$ has a convection condition with heat transfer coefficient h_{cold} and sink temperature $\bar{T}_{\text{water}}$. Applying these boundary conditions gives the 1D temperature field as

$$T_{1D}(x) = \begin{cases} \bar{T}_{\text{water}} + q_{\text{hot}}\left(\dfrac{1}{h_{\text{cold}}} + \dfrac{d_{\text{plate}}}{k_{\text{mould}}} + \dfrac{d_{\text{coat}} - x}{k_{\text{coat}}}\right) & \text{if } 0 \le x \le d_{\text{coat}} \\ \bar{T}_{\text{water}} + q_{\text{hot}}\left(\dfrac{1}{h_{\text{cold}}} + \dfrac{d_{\text{plate}} + d_{\text{coat}} - x}{k_{\text{mould}}}\right) & \text{if } d_{\text{coat}} \le x \le d_{\text{coat}} + d_{\text{plate}}. \end{cases} \tag{2}$$

The 1D temperature solution is shown schematically in Fig. 3, and gives the temperature at key locations in the mould: the hot face temperature $T_{1D,\text{hot}} = T_{1D}(0)$ is

$$T_{1D,\text{hot}} = \bar{T}_{\text{water}} + q_{\text{hot}}\left(\frac{1}{h_{\text{cold}}} + \frac{d_{\text{plate}}}{k_{\text{mould}}} + \frac{d_{\text{coat}}}{k_{\text{coat}}}\right), \tag{3}$$

and the cold face temperature $T_{1D,\text{cold}} = T_{1D}\left(d_{\text{coat}} + d_{\text{plate}}\right)$ is

$$T_{1D,\text{cold}} = \bar{T}_{\text{water}} + \frac{q_{\text{hot}}}{h_{\text{cold}}}. \tag{4}$$

A thermocouple with depth d_{TC} beneath the hot face has temperature $T_{1D,\text{TC}} = T_{1D}(d_{\text{TC}})$, or

$$T_{1D,\text{TC}} = \bar{T}_{\text{water}} + q_{\text{hot}}\left(\frac{1}{h_{\text{cold}}} + \frac{d_{\text{plate}} + d_{\text{coat}} - d_{\text{TC}}}{k_{\text{mould}}}\right). \tag{5}$$

2.2. Cold face model

The cold face of the mould is treated with a convection condition with heat transfer coefficient h_{cold} and sink temperature $\bar{T}_{\text{water}}$. The water flowing in the cooling channels causes a nominal HTC of h_{water} that is modified to account for other phenomena in the water channels. Heat is extracted at the cold face by convection from the roots of the channels, and by combined conduction through the bulk of and convection along the lateral surfaces of the fins. These two heat extraction paths combine to provide a cold face HTC of

$$h_{\text{cold}} = \left(\frac{w_c}{p_c}\right)h_{\text{roots}} + \left(1 - \frac{w_c}{p_c}\right)h_{\text{fins}}, \tag{6}$$

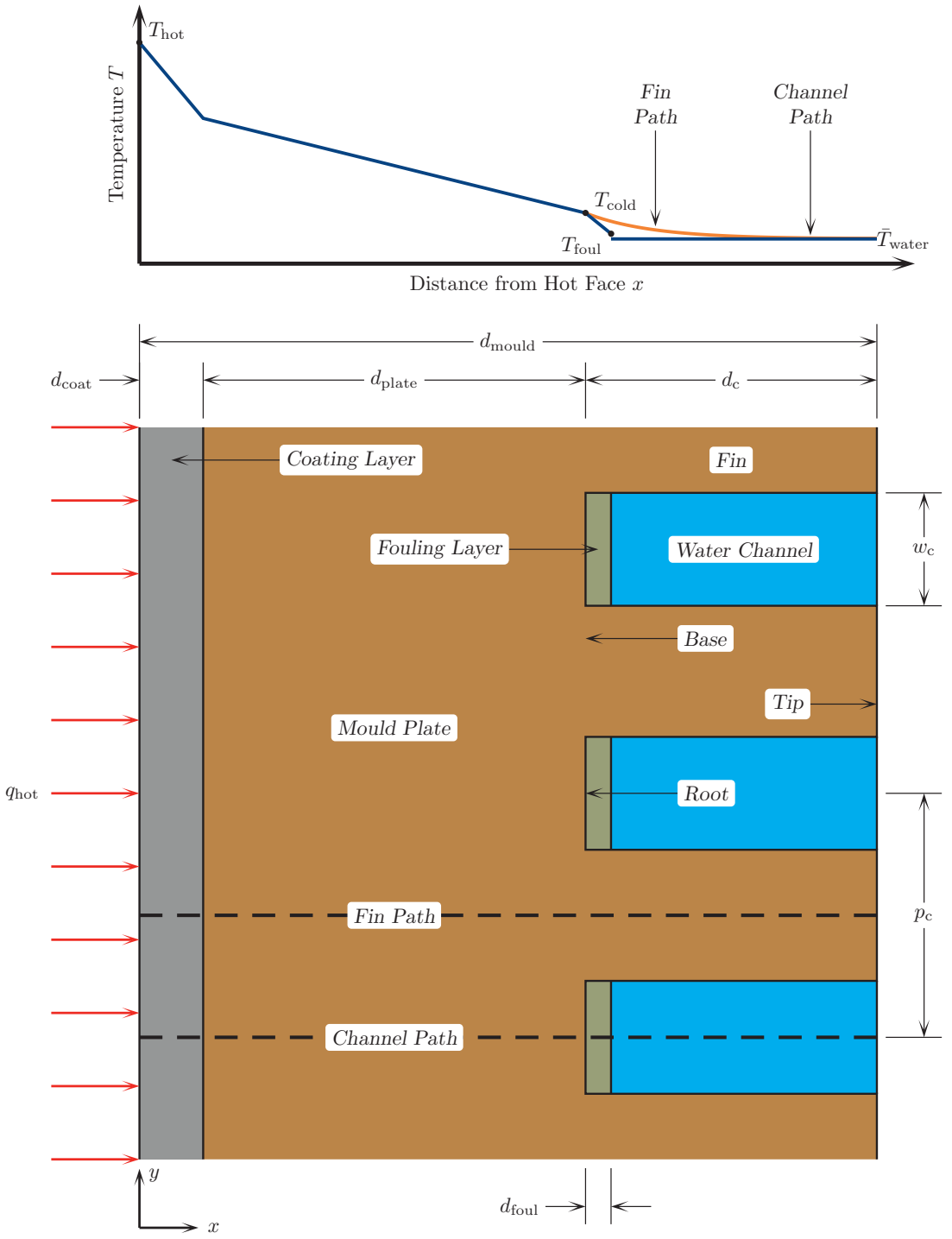

Fig. 3. Mould geometry used for developing the reduced-order model and 1D temperature solution.

where h_{roots} and h_{fins} are the HTCs for the root surfaces and the fins [19].

The heat transfer coefficient for the channel roots h_{roots} is the nominal water HTC h_{water} reduced by the effects of a thin layer of fouling material with thickness d_{foul} and thermal conductivity k_{foul} according to

$$\frac{1}{h_{roots}} = \frac{1}{h_{water}} + \frac{d_{foul}}{k_{foul}}. \tag{7}$$

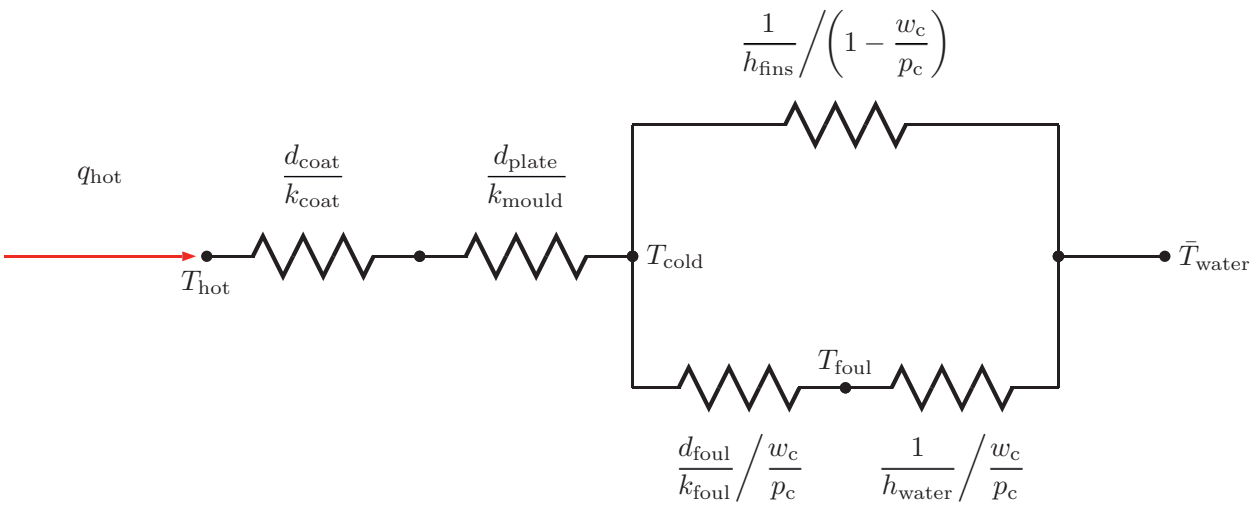

Fig. 4. Thermal resistor model for the one-dimensional mould.

The thickness of the fouling layer is assumed, realistically, to be small compared to the channel depth, *i.e.*, $d_{\text{foul}} / d_c \ll 1$, as to not affect significantly the cooling water flow rate. As the thickness of the fouling layer increases more heat flows into the fins, which is a 2D effect that is not captured by this model. Fouling layers can form on the surface of the water channels as deposits of impurities in the cooling water, usually carbonates, silicates, salts, and oxides, especially if the surface temperature exceeds the boiling temperature of the water. These deposits typically are 20–40 μm thick [68]. With a typical thermal conductivity of about 1 W/(m·K), a 5 μm fouling layer would increase the mould temperatures by about 20 °C, which is consistent with calculations reported elsewhere [68]. This increase in mould temperature makes boiling and further fouling more likely, and changes the heat transfer across the interfacial gap. This model of mould heat transfer can calculate these effects accurately for thin fouling layers.

The mould copper between water channels is assumed to act as a rectangular Murray–Gardner fin with an insulated tip, giving a heat transfer coefficient of [69]

$$h_{\text{fins}} = \frac{k_{\text{mould}}}{d_c} \beta \tanh(\beta) \tag{8}$$

$$\beta = \frac{h_{\text{water}}}{k_{\text{mould}}} d_c \Big/ \sqrt{\frac{h_{\text{water}}}{k_{\text{mould}}} \frac{p_c - w_c}{2}}.$$

The fin tip is insulated because of the assumption that all heat from the steel is removed by the cooling water. Further, in practice the fins often are long enough that the tip temperature is approximately the water temperature, so the small temperature gradient across the interface between the fin tip and waterbox drives a very small heat flow relative to the forced convection along the fin and root surfaces. The analysis behind Eq. (8) assumes that the fin has uniform cross-section and material properties, and that the fin is thin, *i.e.*, $(p_c - w_c)/d_c \ll 1$. A more physical argument is that the fin-thickness Biot number, $h_{\text{water}}(p_c - w_c)/(2k_{\text{mould}})$ is small. In practice, both the fin aspect ratio and the fin-thickness Biot number are about 1/3, so the 2D heat transfer within and at the base of the fins may be significant.

A needed quantity is the perimeter-average temperature of the water channel, $T_{c,\text{ avg}}$. The root of the water channel has a length of w_c and uniform temperature of

$$T_{\text{foul}} = \bar{T}_{\text{water}} + \frac{h_{\text{roots}}}{h_{\text{cold}}} \frac{q_{\text{hot}}}{h_{\text{water}}}, \tag{9}$$

which reduces to the cold face temperature $T_{1D,\text{ cold}}$ when $d_{\text{foul}} = 0$. The top of the water channel has a length of w_c and uniform temperature of $\bar{T}_{\text{water}}$. The two sides of the water channel have a length of d_c and a temperature profile of [69]

$$\frac{T_{\text{fins}}(x') - \bar{T}_{\text{water}}}{T_{\text{base}} - \bar{T}_{\text{water}}} = \frac{1}{\cosh(\beta)} \cosh\left(\beta\left(1 - \frac{x'}{d_c}\right)\right), \tag{10}$$

where $x' = x - \left(d_{\text{coat}} + d_{\text{plate}}\right)$ is the distance from the base of the fin, where the temperature is that of the cold face, *i.e.*, $T_{\text{base}} = T_{1D,\text{cold}}$. The perimeter-average temperature of the rectangular water channel then is

$$T_{\mathrm{c,avg}} = \frac{1}{2(w_\mathrm{c}+d_\mathrm{c})}\left(\int_0^{w_\mathrm{c}} T_{\mathrm{foul}}\,\mathrm{d}y + 2\int_0^{d_\mathrm{c}} T_{\mathrm{fins}}(x')\,\mathrm{d}x' + \int_0^{w_\mathrm{c}} \bar{T}_{\mathrm{water}}\,\mathrm{d}y\right)$$
$$= \bar{T}_{\mathrm{water}} + \frac{p_\mathrm{c}}{2(w_\mathrm{c}+d_\mathrm{c})}\frac{q_{\mathrm{hot}}}{h_{\mathrm{water}}}. \tag{11}$$

The water HTC h_{water} itself is calculated with a forced-internal-flow empirical correlation. For example, the Sleicher and Rouse [70] model,

$$\mathrm{Nu} = 5 + 0.015\,\mathrm{Re}^{a_1}\,\mathrm{Pr}^{a_2} \tag{12}$$
$$a_1 = 0.88 - \frac{0.24}{4+\mathrm{Pr}}$$
$$a_2 = \frac{1}{3} + 0.5\exp(-0.6\,\mathrm{Pr}),$$

is used in this work because of its accurate fit, on average about 7% error [70], with measurements. The Nusselt number, $\mathrm{Nu} = h_{\mathrm{water}}D_{\mathrm{h,c}}/k_{\mathrm{water}}$, from which the water HTC h_{water} is calculated, is evaluated at the bulk temperature of the water $\bar{T}_{\mathrm{water}}$. The Prandtl number, $\mathrm{Pr} = \mu_{\mathrm{water}}c_{p,\mathrm{water}}/k_{\mathrm{water}}$, is evaluated at the perimeter-average temperature of the water channel surface $T_{\mathrm{c,\,avg}}$. The Reynolds number, $\mathrm{Re} = \rho_{\mathrm{water}}\bar{v}_{\mathrm{water}}D_{\mathrm{h,c}}/\mu_{\mathrm{water}}$, is evaluated at the "film" temperature $T_{\mathrm{film}} = \frac{1}{2}\left(\bar{T}_{\mathrm{water}} + T_{\mathrm{c,avg}}\right)$. Eq. (12) is valid for $10^{-1} \le \mathrm{Pr} \le 10^5$ and $10^4 \le \mathrm{Re} \le 10^6$. The hydraulic diameter, defined as four times the cross-sectional area divided by the perimeter length, of the rectangular water channels is $D_{\mathrm{h,c}} = 2w_\mathrm{c}d_\mathrm{c}/(w_\mathrm{c}+d_\mathrm{c})$. The average speed of the water in the channel, $\bar{v}_{\mathrm{water}} = Q_{\mathrm{water}}/A_{\mathrm{c,total}}$, is calculated from the total volumetric flow rate of the cooling water Q_{water} measured in the plant and the total cross-sectional area $A_{\mathrm{c,\,total}}$ of all water channels in the mould. The water properties vary with temperature T in °C according to[1]

$$k_{\mathrm{water}}(T) = 0.59 + 0.001\,T, \tag{13}$$

$$\rho_{\mathrm{water}}(T) = 1000.3 - 0.040286\,T - 0.0039779\,T^2, \tag{14}$$

$$c_{p,\mathrm{water}}(T) = 4215.0 - 1.5594\,T + 0.015234\,T^2, \tag{15}$$

$$\mu_{\mathrm{water}}(T) = 2.062e-9\rho_{\mathrm{water}}10^{\frac{792.42}{T+273.15}}, \tag{16}$$

with thermal conductivity k_{water} in W/(m · K), mass density ρ_{water} in kg/m^3, isobaric specific heat capacity $c_{p,\,\mathrm{water}}$ in J/kg · K, and dynamic shear viscosity μ_{water} in Pa · s. For conditions typical of continuous casting, Pr ≈ 4 and Re ≈ 1.5 × 10^5, so Eq. (12) safely gives Nu ≈ 300. Eq. (12) assumes that the flow in the channel is fully developed, which for continuous casting requires that the position of the meniscus of the molten metal occurs lower in the mould than the entry length of the channel, or with the usual liberal estimate that $\ell_{\mathrm{meniscus}}/D_{\mathrm{h,\,c}} > 10$.

Boiling in the water channels should be avoided because of the possible formation of fouling material and reduction of heat transfer. A simple evaluation of the risk of boiling [27,38] is to compare the water temperature, in particular at the channel roots, against the boiling temperature of water. Since the water in the mould is pressurised, the boiling temperature of water $T_{\mathrm{boil,\,water}}(p)$ is computed with [72]

$$T_{\mathrm{boil,water}} = \frac{1810.94}{8.14019 - \log_{10}(7500.69\,p)} - 244.485. \tag{17}$$

Eq. (17) expects the absolute pressure p in MPa and gives the boiling temperature in °C.

2.3. Cooling water temperature change

The temperature change of the cooling water is an important quantity in the validation of mould heat transfer models because it is an indirect measurement of the total energy removed from the strand by the mould. This section presents the calculation of the temperature change of the cooling water, in a manner that is consistent with the reduced-order model.

Assuming that the water moves mostly in the axial (z) direction of the water channel with average speed $\bar{v}_{\mathrm{water}}$, the scaled [67] steady energy equation is

$$\frac{\partial\theta_{\mathrm{water}}}{\partial z^*} = \frac{1}{\mathrm{Pe}_{\mathrm{water}}\frac{D_{\mathrm{h,c}}}{\ell_\mathrm{c}}}\left(\frac{\partial^2\theta_{\mathrm{water}}}{\partial x^{*2}} + \frac{\partial^2\theta_{\mathrm{water}}}{\partial y^{*2}} + \left(\frac{D_{\mathrm{h,c}}}{\ell_\mathrm{c}}\right)^2\frac{\partial^2\theta_{\mathrm{water}}}{\partial z^{*2}}\right), \tag{18}$$

where $\theta_{\mathrm{water}} = \left(T_{\mathrm{water}} - T_{\mathrm{water,min}}\right)/\left(T_{\mathrm{water,max}} - T_{\mathrm{water,min}}\right)$ is the water temperature T_{water} scaled by the largest and smallest temperatures in the channel $T_{\mathrm{water,\,max}}$ and $T_{\mathrm{water,\,min}}$, $x^* = x/D_{\mathrm{h,c}}$, $y^* = y/D_{\mathrm{h,c}}$, and $z^* = z/\ell_\mathrm{c}$ are the coordinates

[1] Eqs. (13)–(16) are simple fits to standard reference data [71]. More accurate correlations are available in the literature, but the accuracy of this model for the water HTC h_{water} is not limited by the material properties.

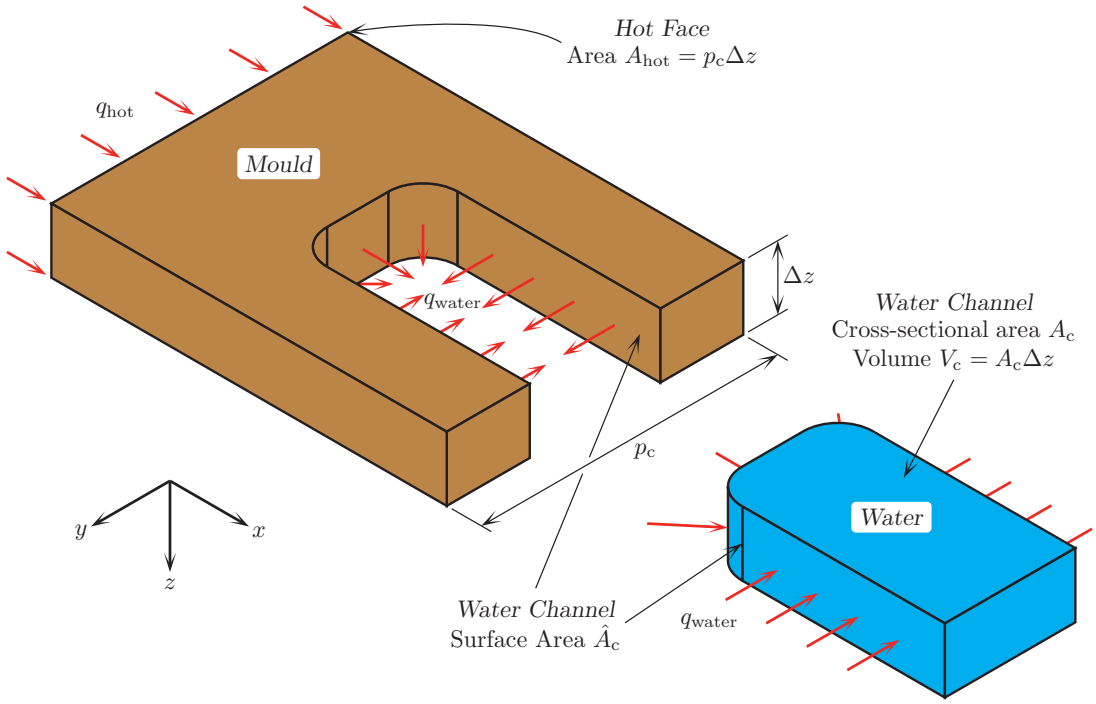

Fig. 5. Domain for analysing the cooling water temperature change.

scaled by the hydraulic diameter $D_{h,\,c}$ and length ℓ_c of the water channel, $\mathrm{Pe}_{water} = \bar{v}_{water} D_{h,c} / \alpha_{water}$ is the Péclet number of the flow in the water channel, and $\alpha_{water} = k_{water} / \rho_{water} c_{p,water}$ is the thermal diffusivity of the water. Eq. (18) indicates that the heat conducted in the axial (z) direction is negligible relative to the heat conducted in the transverse directions because of the small aspect ratio of the channel, *i.e.*, $D_{h,\,c} / \ell_c \ll 1$. Further, since the aspect-ratio–modified Péclet number is large, *i.e.*, $\mathrm{Pe}_{water} D_{h,\,c} / \ell_c \gg 1$, the heat conduction is negligible relative to the energy transported by the bulk motion of the water. Eq. (18) then indicates that the water temperature can be taken as uniform over the entire channel, so an alternative approach must be used to analyse the temperature change of the water.

Instead, consider a transverse slice with thickness $\Delta z > 0$ of a water channel and the surrounding mould, as shown in Fig. 5. The integral form of the steady energy equation for the water, assuming no boiling, in the transverse slice is

$$\int_{V_c} \rho_{water} c_{p,water} v_{water} \frac{\partial T_{water}}{\partial z} \, \mathrm{d}V = - \int_{\hat{A}_c} -q_{water} \, \mathrm{d}A, \tag{19}$$

where V_c is the volume of the slice of water, $\hat{A}_c$ is the surface area of the water channel in the slice, and $q_{water} > 0$ is the heat flux into the water. Assuming that all heat supplied to the mould is removed by the cooling water, the integral form of the steady energy equation for the mould in the transverse slice is

$$0 = - \int_{A_{hot}} -q_{hot} \, \mathrm{d}A - \int_{\hat{A}_c} q_{water} \, \mathrm{d}A, \tag{20}$$

where the area of the hot face in the transverse slice is $A_{hot} = p_c \Delta z$. If the heat flux on the hot face is uniform across the slice, then the heat input to the water is

$$\int_{\hat{A}_c} q_{water} \, \mathrm{d}A = q_{hot} p_c \Delta z \tag{21}$$

regardless of the shape of the water channel. The hot face heat flux q_{hot} is uniform for an arbitrarily small Δz and a sufficiently large water channel width-to-pitch ratio w_c / p_c. The volume integral over the water in Eq. (19) is evaluated by defining the water bulk temperature $\bar{T}_{water}$ as the temperature that satisfies

$$\rho_{water}\left(\bar{T}_{water}\right) c_{p,water}\left(\bar{T}_{water}\right) \bar{v}_{water} \bar{T}_{water} A_c = \int_{A_c} \rho_{water} c_{p,water} v_{water} T_{water} \, \mathrm{d}A, \tag{22}$$

i.e., $\bar{T}_{water}(z)$ is the internal-energy–weighted average temperature over a plane perpendicular to the flow of the water with cross-sectional area A_c. Eq. (22) allows the volume integral in Eq. (19) to be evaluated for small Δz as

$$\int_{V_c} \rho_{water} c_{p,water} v_{water} \frac{\partial T_{water}}{\partial z} \, \mathrm{d}V = \rho_{water} c_{p,water} \bar{v}_{water} \frac{\mathrm{d}\bar{T}_{water}}{\mathrm{d}z} A_c \Delta z, \tag{23}$$

with ρ_{water} and $c_{p,\text{ water}}$ on the right side of the equation evaluated at $\bar{T}_{\text{water}}$. Combining Eqs. (19), (21), and (23) and dividing out the Δz gives the differential equation that describes the evolution of the water bulk temperature in one channel as

$$\frac{\mathrm{d}\bar{T}_{\text{water}}}{\mathrm{d}z} = \frac{q_{\text{hot}} p_{\text{c}}}{\rho_{\text{water}} c_{p,\text{water}} \bar{v}_{\text{water}} A_{\text{c}}}. \tag{24}$$

The above arguments are extended to find the temperature change of all cooling water in the mould. The heat flux from the steel is applied over the width of the strand w_{strand} rather than a single channel pitch. The heat leaves the mould through all water channels with total cross-sectional area $A_{\text{c, total}}$, regardless of channel shape and pitch; however, the average water speed in each channel must be about the same value. The temperature evolution of the total water then is described by

$$\frac{\mathrm{d}\bar{T}_{\text{water}}}{\mathrm{d}z} = \frac{q_{\text{hot}} w_{\text{strand}}}{\rho_{\text{water}} c_{p,\text{water}} \bar{v}_{\text{water}} A_{\text{c,total}}}. \tag{25}$$

The water temperature at an arbitrary distance down the mould z is found by numerical integration of Eq. (25) with the initial condition $\bar{T}_{\text{water}}(0)$ measured in the plant at the top of the mould. The ROM must match the measured water temperature at the bottom of the mould $\bar{T}_{\text{water}}(\ell_{\text{mould}})$ as part of model validation and/or calibration. This calculation of water temperature change works equally well in counterflow configurations, where the cooling water flows opposite to the casting direction, but with $\bar{v}_{\text{water}} < 0$.

3. Three-dimensional mould model: snapshot model

The snapshot model needed to calibrate the ROM developed in this work is a 3D analysis of the small, periodic and symmetric "unit cell" of the mould highlighted in Fig. 2. The temperature field in this 3D model of the mould $T_{\text{3D}}(\boldsymbol{x})$ is determined by solving the steady heat-conduction equation,

$$0 = \nabla \cdot (k_{\text{mould}} \nabla T_{\text{3D}}), \tag{26}$$

where k_{mould} is the isotropic thermal conductivity of the mould. The temperature dependence of the thermal conductivity of mould copper alloys has a negligible effect on the calculated temperature field [35], so the governing equation can be simplified to the Laplacian equation to avoid nonlinear complications. A uniform heat flux $q_{\text{hot}} > 0$ is applied to the mould hot face as

$$-k_{\text{mould}} \nabla T_{\text{3D}} \cdot \boldsymbol{n} = -q_{\text{hot}}, \tag{27}$$

where $\boldsymbol{n}$ is the outward-pointing unit normal vector of the surface. The heat flux from the strand depends nonlinearly on the conductive and radiative properties of the material in the gap between the strand and the mould, but this model needs only to relate the mould temperatures to some arbitrary heat flux. Energy is extracted from the water channel surfaces by a uniform convection condition,

$$-k_{\text{mould}} \nabla T_{\text{3D}} \cdot \boldsymbol{n} = h_{\text{water}} \left(T_{\text{3D}} - \bar{T}_{\text{water}} \right), \tag{28}$$

where T_{3D} here is the channel surface temperature, h_{water} is the heat transfer coefficient (HTC) of the cooling water, and the sink temperature is taken as the bulk temperature of the cooling water $\bar{T}_{\text{water}}$. All other faces are insulated, *i.e.*, $-k_{\text{mould}} \nabla T_{\text{3D}} \cdot \boldsymbol{n} = 0$, because of symmetry or the assumption that heat is removed only by the cooling water. Any other features of the mould, such as a coating layer on the hot face or fouling material in the cooling channels, should be included in this snapshot model. This boundary-value problem is solved readily with the finite element method, owing to the ability of the method to handle easily the geometric features of a continuous casting mould. Modern computers can solve this linear heat conduction problem in seconds, depending on mesh resolution.

The temperatures in this snapshot model are computed using the actual geometry of the mould, including the coating and fouling layer thicknesses, and values reasonable for the process of: the hot face heat flux $q^{\diamond}_{\text{hot}}$; the water channel HTC $h^{\diamond}_{\text{water}}$; the bulk temperature of the cooling water $\bar{T}^{\diamond}_{\text{water}}$; and the thermal conductivities of the mould $k^{\diamond}_{\text{mould}}$, coating layer $k^{\diamond}_{\text{coat}}$, and fouling layer $k^{\diamond}_{\text{foul}}$. The specific values chosen here, indicated with the superscript diamonds, also are used in the ROM calibration discussed in Section 4, because the calibration method forces the temperature at specific locations in the 1D model to match the corresponding temperatures in the 3D model for identical boundary conditions and material properties. The geometry of the coating and fouling layers also must be averaged for the corresponding parameters $d^{\diamond}_{\text{coat}}$ and $d^{\diamond}_{\text{foul}}$ for the ROM calibration. The four temperatures of interest in this snapshot model used for the calibration are:

- the average hot face temperature, $T_{\text{3D, hot}}$, which is used in calculations of the strand-mould interfacial heat transfer,
- the average water channel surface temperature, $T_{\text{3D, c, avg}}$, which is needed to calculate the HTC for the water convection,
- the maximum water channel surface temperature, $T_{\text{3D, c, max}}$, usually occurring at the channel root, which is used to evaluate the risk of boiling the cooling water, and
- the average thermocouple face temperature, $T_{\text{3D, TC}}$, which is an important validation and/or calibration point in models of mould heat transfer.

The averaging is carried out over the appropriate surfaces indicated in Fig. 2.

4. Reduced-order model parameter calibration

The thirteen parameters in the reduced-order model of mould heat transfer presented in Section 2 are:

- the boundary conditions: the hot face heat flux q_{hot}, and the water heat transfer coefficient h_{water} and bulk temperature $\bar{T}_{\text{water}}$,
- the material properties: the coating, mould, and fouling thermal conductivities k_{coat}, k_{mould}, and k_{foul}, and
- the geometric parameters: the coating, mould plate, and fouling thicknesses d_{coat}, d_{plate}, and d_{foul}, the thermocouple position d_{TC}, and the water channel width w_{c}, depth d_{c}, and pitch p_{c}.

The philosophy for calibrating the ROM is to adjust parameters that do not change when the model is used: for a continuous casting mould, the geometric parameters are constant. The assumptions on the nature of the heat flow in the 1D temperature solution also suggest that the geometric parameters are good candidates for calibration. The coating and fouling layer thermal conductivities and thicknesses are not calibrated because these layers are so thin that they act like 1D thermal resistances regardless of the complexity of the model, and because these thicknesses change over the life of the mould. The material properties like the thermal conductivities could be calibrated, but this was not done in this work. The five remaining constant parameters, the mould plate thickness d_{plate}, the thermocouple depth d_{TC}, and the channel width w_{c}, depth d_{c}, and pitch p_{c}, are calibrated according to the methodology presented in this section, so that the ROM of the mould has the same heat extraction characteristics as the actual mould, and so that the ROM can match the four key temperatures in the 3D snapshot model discussed in Section 3.

4.1. Water channel geometry

The reduced-order model water channel geometry is calibrated to provide the same heat extraction characteristics as the actual mould. The water channels in the ROM must have the same cross-sectional area as the actual channels A_{actual}, *i.e.*,

$$w_{\text{c}} d_{\text{c}} = A_{\text{actual}}, \tag{29}$$

to maintain the volumetric flow rate of the cooling water. The water channels in the ROM also must have the same hydraulic diameter as the actual channels $D_{\text{h, actual}}$, *i.e.*,

$$2\frac{w_{\text{c}} d_{\text{c}}}{w_{\text{c}} + d_{\text{c}}} = D_{\text{h,actual}}, \tag{30}$$

to maintain the value of the water HTC from Eq. (12) or another correlation for the Nusselt number. Solving Eqs. (29) and (30) together gives the ROM channel width w_{c} and depth d_{c} as

$$w_{\text{c}}, d_{\text{c}} = \frac{A_{\text{actual}}}{D_{\text{h,actual}}}\left(1 \pm \sqrt{1 - \frac{D_{\text{h,actual}}^2}{A_{\text{actual}}}}\right). \tag{31}$$

Both solutions of Eq. (31) are real and positive if $A_{\text{actual}} \geq D_{\text{h,actual}}^2$; otherwise some manual intervention is necessary [36]. The aspect ratio of the actual channels determines which solution is w_{c} and which is d_{c}, subject to $w_{\text{c}} < p_{\text{c}}$. If the mould employs channels with different geometries, then the values of A_{actual} and $D_{\text{h, actual}}$ are taken as their respective averages over all channels in the mould, or, separate reduced-order models can be developed for different regions of the mould, depending on the interest of the modeller.

The ROM channel pitch p_{c} is calibrated by requiring that the simulated and physical moulds have the same amount of cooling water flowing per unit width of the mould, *i.e.*,

$$\frac{A_{\text{c}}}{p_{\text{c}}} = \frac{A_{\text{c,total}}}{w_{\text{mould}}}, \tag{32}$$

where the ROM water channel cross-sectional area $A_{\text{c}} = w_{\text{c}} d_{\text{c}}$ is calculated with the calibrated dimensions from Eq. (31), and $A_{\text{c, total}}$ is the total channel cross-sectional area contained within a chosen width w_{mould} of the mould. In many cases it is sufficient to use the geometry of the snapshot model domain in Section 3 as the basis for this calculation. Eq. (32) is an accurate approximation of the slope of the best-fit line through a curve describing the cumulative water channel cross-sectional area across the width of the mould, which was used in previous work [27].

4.2. Mould plate thickness

The calibrated mould plate thickness d_{plate} is found by requiring the 1D hot face temperature to be the average hot face temperature from the ± finite-element model, *i.e.*, $T_{\text{1D,hot}} = T_{\text{3D,hot}}$. Manipulating the expression for the 1D hot face temperature, Eq. (3), gives a mould plate thickness of

$$d_{\text{plate}} = \frac{k_{\text{mould}}^{\diamond}}{q_{\text{hot}}^{\diamond}}\left(T_{\text{3D,hot}} - \bar{T}_{\text{water}}^{\diamond}\right) - k_{\text{mould}}^{\diamond}\left(\frac{1}{h_{\text{cold}}^{\diamond}} + \frac{d_{\text{coat}}^{\diamond}}{k_{\text{coat}}^{\diamond}}\right), \tag{33}$$

where $h^{\diamond}_{\text{cold}}$ is calculated with Eq. (6) using the calibrated channel geometry from Section 4.1, and the other "diamond" values are the same as used in the snapshot model. Some phenomena related to strand-mould interfacial heat transfer depend on the mould hot face temperature, and this calibrated plate thickness ensures that $T_{1\text{D, hot}}$ is computed accurately. Some previous work [29,34] proposed effective plate thicknesses, but none could produce consistently the correct hot face temperature. The sensitivity of this calibrated plate thickness to the "diamond" values is explored in Section 6.

4.3. Cold faces

The 1D model has a unique "cold face" temperature, predicted by Eq. (4), but the actual mould has cold face surfaces with several temperatures at different locations that are of practical interest. To accommodate these multiple temperatures, new "distances to the cold face" are defined such that the 1D model temperature exactly matches the temperature predicted with the snapshot model presented in Section 3. One such cold face at $d_{\text{c, avg}}$ gives the average water channel temperature, which is used to calculate the water HTC with Eq. (12). The distance is chosen such that $T_{1\text{D}}\left(d_{\text{c,avg}}\right) = T_{\text{3D,c,avg}}$, and rearranging Eq. (2) gives

$$d_{\text{c,avg}} = \frac{k^{\diamond}_{\text{mould}}}{q^{\diamond}_{\text{hot}}}\left(T_{\text{3D,hot}} - T_{\text{3D,c,avg}}\right) + d^{\diamond}_{\text{coat}}\left(1 - \frac{k^{\diamond}_{\text{mould}}}{k^{\diamond}_{\text{coat}}}\right), \tag{34}$$

where $T_{\text{3D,c,avg}}$ is the average temperature of the channel surfaces in the 3D snapshot model. Another cold face at $d_{\text{c, max}}$ calculates the maximum water channel temperature, *i.e.*, $T_{1\text{D}}(d_{\text{c,max}}) = T_{\text{3D,c,max}}$, which is used to evaluate the risk of boiling with Eq. (17). Similar to Eq. (34), this distance is

$$d_{\text{c,max}} = \frac{k^{\diamond}_{\text{mould}}}{q^{\diamond}_{\text{hot}}}\left(T_{\text{3D,hot}} - T_{\text{3D,c,max}}\right) + d^{\diamond}_{\text{coat}}\left(1 - \frac{k^{\diamond}_{\text{mould}}}{k^{\diamond}_{\text{coat}}}\right), \tag{35}$$

where $T_{\text{3D,c,max}}$ is the maximum temperature of the channel surfaces in the 3D snapshot model. The distances from the hot face of these two cold face locations are used with the 1D temperature solution, Eq. (2), instead of the model-consistent expressions for the channel average and maximum temperatures, Eqs. (11) and (9), for increased accuracy. The two cold faces defined here are of general interest, but in principle the average and maximum surface temperatures of each water channel, or any other temperature of interest, can be calculated with this approach of extra calibration steps to match each of the multiple cold face temperatures.

4.4. Mould thermocouples

The mould thermocouples in the ROM are calibrated to account for the geometric effect of the thermocouple hole, and to account for the heat lost along the long thermocouple wires. The geometric effect can be significant: the temperature from Eq. (5) can under-predict the thermocouple temperature from the 3D model, by as much as 50°C [29,36], or about 25%, depending on the geometry. Following similar arguments as in calibrating the cold face temperatures, the calibrated thermocouple position d_{TC} is found by manipulating Eq. (5) with $T_{\text{1D,TC}} = T_{\text{3D,TC}}$, giving

$$d_{\text{TC}} = \frac{k^{\diamond}_{\text{mould}}}{q^{\diamond}_{\text{hot}}}\left(T_{\text{3D,hot}} - T_{\text{3D,TC}}\right) + d^{\diamond}_{\text{coat}}\left(1 - \frac{k^{\diamond}_{\text{mould}}}{k^{\diamond}_{\text{coat}}}\right), \tag{36}$$

where $T_{\text{3D, TC}}$ is the average temperature of the thermocouple face in the 3D snapshot model.

Eq. (36) corrects for the geometric inaccuracies of the thermocouple temperature, but in practice is not the only correction needed to match thermocouple measurements. Measured thermocouple temperatures often read low because of the contact resistance between the thermocouple bead and the mould. Heat is lost through conduction and convection along the length of the thermocouple wires, which also affects the thermocouple reading. Assuming that the thermocouple wires behave as long circular pin-fins, the heat loss q_{TC} is

$$q_{\text{TC}} = \frac{k_{\text{TC}}}{D_{\text{TC}}/2}\sqrt{\frac{h_{\text{wire}}D_{\text{TC}}}{k_{\text{TC}}}}\left(T_{\text{TC}} - T_{\text{amb}}\right), \tag{37}$$

where D_{TC} and k_{TC} are the diameter and thermal conductivity of the thermocouple wire, which is submersed in a fluid of temperature T_{amb} that causes a convection coefficient of h_{wire}. The wire heat transfer coefficient h_{wire} is intended to be a tuning parameter, and should be about 5 kW/(m^2 · K) if the ambient medium is water or about 0.1 kW/(m^{2}K) for air. This energy lost along the thermocouple wires is treated as a local adjustment to the thermocouple temperature because the heat leaving the mould through the thermocouples is small relative to the heat leaving through the water channels:

$$T'_{\text{TC}} = T_{\text{TC}} + q_{\text{TC}}\frac{d_{\text{gap}}}{k_{\text{gap}}}, \tag{38}$$

where T_{TC} is the predicted thermocouple temperature from Eq. (5) using the calibrated thermocouple depth d_{TC} from Eq. (36), and d_{gap} and k_{gap} are the size and thermal conductivity of the gap between the thermocouple and the mould. The thermal conductivity of the gap should be about 1.25 W/(m · K) for a thermal paste or about 0.04 W/(m · K) for dry air. The gap size typically is on the order of 0.01–0.1 mm, and is intended to be another tuning parameter. This approach of calibrating mould thermocouple temperatures has been demonstrated elsewhere [22,26].

Table 1
Example mould geometry temperatures.

Temperature (°C)	Mould A [29]		Mould B [29]		Mould C [36]		Mould D [27]	
	Uncalibrated	Calibrated	Uncalibrated	Calibrated	Uncalibrated	Calibrated	Uncalibrated	Calibrated
Hot face, T_{hot}	317.5	323.8	187.9	192.6	276.3	282.5	242.1	245.7
Cold face, T_{cold}	79.36		58.09		96.33		87.67	
Channel maximum, $T_{c,max}$		107.0		72.54		124.1		96.76
Channel average, $T_{c,avg}$	59.25	63.52	37.68	39.42	61.92	66.33	60.32	58.98
Thermocouple, T_{TC}	127.0	172.0	82.12	103.8	147.8	179.6	130.9	146.7

4.5. Summary of calibration procedure

The overall calibration procedure for the ROM of a continuous casting mould is:

1. Mould geometry calibration, as discussed in this work.
   (a) Select process-appropriate values of $q^{\diamond}_{hot}$, $h^{\diamond}_{water}$, $\bar{T}^{\diamond}_{water}$, $k^{\diamond}_{mould}$, $k^{\diamond}_{coat}$, and $k^{\diamond}_{foul}$.
   (b) Analyse the 3D snapshot model with exact mould geometry as described in Section 3. Extract from the model the four temperatures $T_{3D,hot}$, $T_{3D,c,avg}$, $T_{3D,c,max}$, and $T_{3D,TC}$.
   (c) Calculate average values of coating and fouling layer thicknesses $d^{\diamond}_{coat}$ and $d^{\diamond}_{foul}$, based on input to the snapshot model.
   (d) Calculate A_{actual} and $D_{h,actual}$ based on blueprint geometry, then calculate w_c and d_c with Eq. (31) and then calculate p_c with Eq. (32).
   (e) Calculate $h^{\diamond}_{cold}$ with Eq. (6).
   (f) Calculate d_{plate} with Eq. (33).
   (g) Calculate $d_{c,avg}$ with Eq. (34).
   (h) Calculate $d_{c,max}$ with Eq. (35).
   (i) Calculate d_{TC} with Eq. (36).
2. Heat flux profile calibration, which is discussed in detail elsewhere [22,36,64]. The heat flux from the strand is affected by many process and physical variables, including: superheat distribution in the liquid, mould oscillation practices, casting speed, slag thermal and mechanical properties, and steel thermal and mechanical properties. The many parameters must be calibrated to match:
   (a) the cooling water temperature change, integrated from Eq. (25),
   (b) the profile of a "breakout shell," the solid husk left over after the molten metal pool is drained [64], and
   (c) the adjusted mould thermocouple temperatures from Eq. (38).
   The mould geometry calibration presented in this work allows reasonable values to be obtained for all variables, *e.g.*, the uncalibrated mould thermocouple temperatures are not consistent with typical values of total heat removal.

5. Example mould geometries

This section demonstrates the reduced-order model calibration process for four wide face mould geometries. This work employs the commercial finite-element software ABAQUS [73] for analysing the 3D snapshot models. Moulds A and B [29] are for conventional "thick-slab" moulds, Mould C [36] is for a thin-slab funnel mould, and Mould D [27] is for a thin-slab mould without a funnel. None of these moulds employ a coating layer. Slices through the snapshot model domains at the centre of the thermocouple hole are shown in Figs. 6–9. These figures also give the results from the 3D model that are necessary for the calibration calculations, as well as the calibrated geometries for the reduced-order models of these moulds. Water channels that are split by a symmetry plane, as on Moulds A and B, have weights of 0.5 in the averaging calculations.

The severity of the adjustment to the channel geometry depends on the shapes and distribution of channels in the physical mould. The mould plate thickness and cold face locations differ about 10% from the blueprint dimensions. Table 1 compares the temperatures from the "uncalibrated" 1D heat-transfer model of the mould using the blueprint geometry, and from the calibrated reduced-order model. The ROM matches the four key temperatures from the 3D snapshot model by construction, and the uncalibrated model under-predicts these temperatures by as much as 26%. Some moulds, such as Mould D, are modelled reasonably well by the uncalibrated 1D model.

6. Sensitivity of mould geometry calibration to model parameters

The reduced-order model is useful only if the boundary conditions can change and the model still is able to calculate the correct temperatures. This section explores the sensitivity of the results of the calibration procedure described in Section 4. The insensitivity to the non-geometric ROM parameters is demonstrated by showing that the calibration procedure gives the same value of the calibrated geometry for different values of the non-geometric parameters.

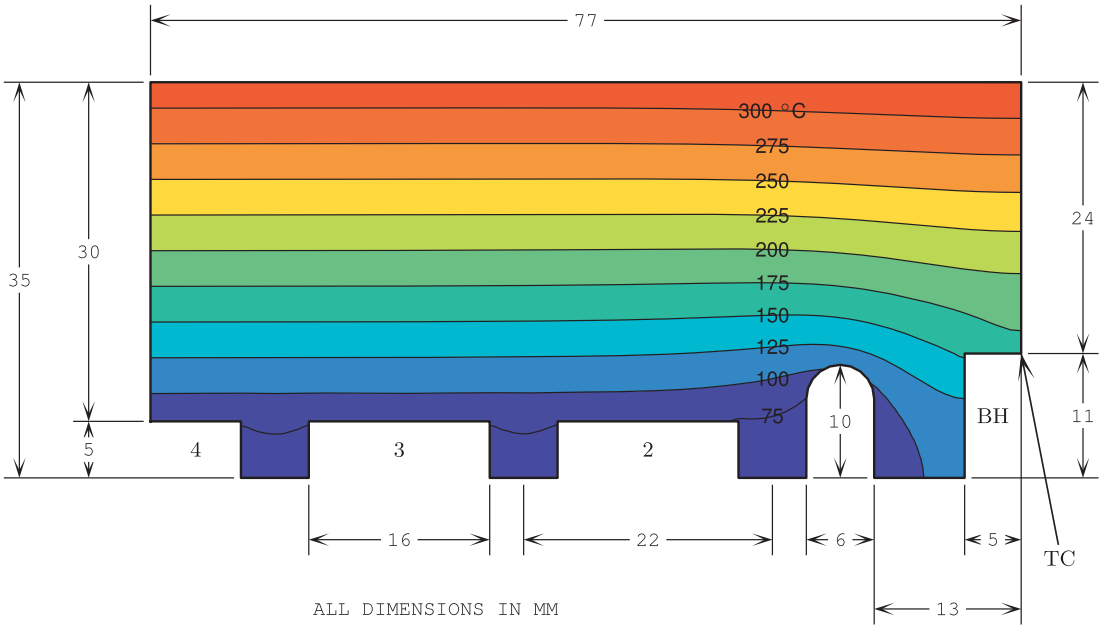

$$k^{\diamond}_{\text{mould}} = 315\,\text{W/(m}\cdot\text{K)}$$
$$q^{\diamond}_{\text{hot}} = 2500\,\text{kW/m}^2$$
$$h^{\diamond}_{\text{water}} = 54\,\text{kW/(m}^2\cdot\text{K)}$$
$$\bar{T}^{\diamond}_{\text{water}} = 35\,^{\circ}\text{C}$$

$$T_{\text{3D,hot}} = 323.8\,^{\circ}\text{C}$$
$$T_{\text{3D,TC}} = 172.0\,^{\circ}\text{C}$$

Channel	A_c mm^2	$D_{h,c}$ mm	$T_{c,avg}$ °C	$T_{c,max}$ °C
1	56.14	7.631	71.86	107.0
2	80.0	7.619	59.20	79.79
3	80.0	7.619	60.52	80.61
4	80.0	7.619	62.50	80.70
Total	256.1			
ROM	73.18	7.623	63.52	107.0

Model	w_c mm	d_c mm	p_c mm	d_{plate} mm	$d_{c,max}$ mm	$d_{c,avg}$ mm	d_{TC} mm
Uncalibrated ROM	16.0	5.0	22.0	30.0			24.0
Calibrated ROM	13.96	5.243	22.0	30.46	27.32	32.79	19.13

Fig. 6. Calibration domain geometry, conditions, and results for Mould A [29].

To provide a scale for the sensitivity of the calibrated geometric parameters, the derivative of the 1D temperature solution, Eq. (2), with respect to the heat load is

$$\frac{\partial T_{\text{1D}}}{\partial q_{\text{hot}}} = \left(\frac{1}{h_{\text{cold}}} + \frac{d_{\text{plate}}}{k_{\text{mould}}}\right) + \left(\frac{q_{\text{hot}}}{k_{\text{mould}}}\frac{\partial d_{\text{plate}}}{\partial q_{\text{hot}}}\right), \tag{39}$$

taking $d_{\text{coat}} = 0$ and $d_{\text{foul}} = 0$ for simplicity. The second term arises because of the dependence of the calibrated mould plate thickness upon the hot face heat flux; this term must be small relative to the first term for the calibrated ROM temperatures to be insensitive to the value of the calibration parameter, or that

$$\left|\frac{\partial d_{\text{plate}}}{\partial q_{\text{hot}}}\right| \ll \frac{k_{\text{mould}}}{q_{\text{hot}} h_{\text{cold}}} + \frac{d_{\text{plate}}}{q_{\text{hot}}}. \tag{40}$$

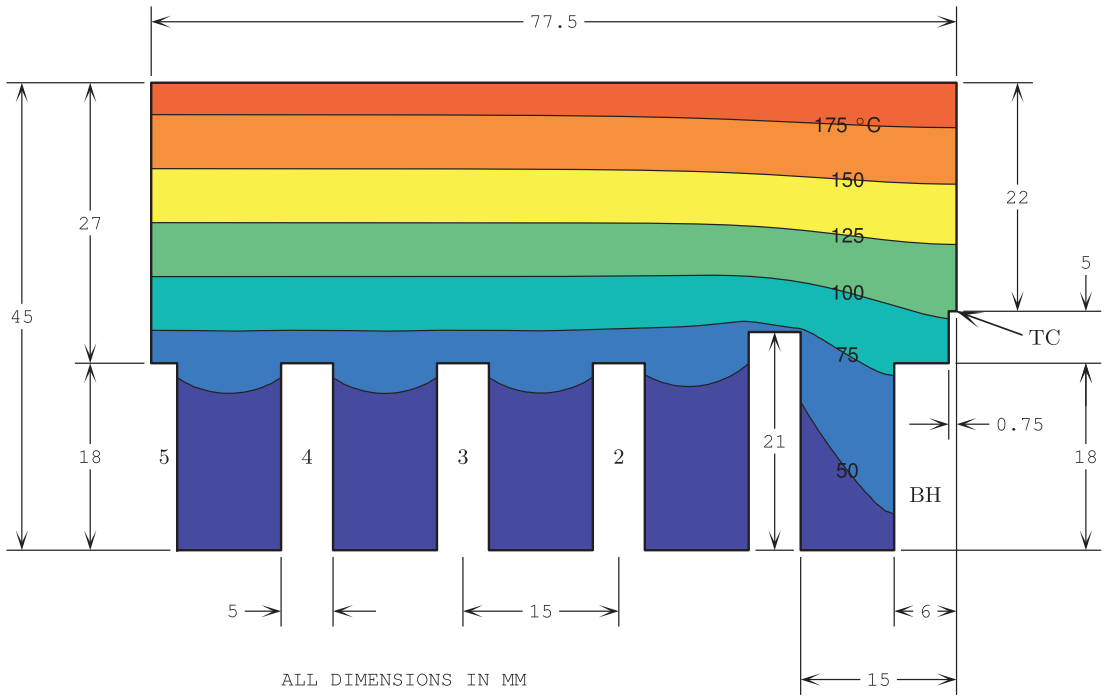

$$k^{\diamond}_{\text{mould}} = 364\,\text{W/(m}\cdot\text{K)}$$
$$q^{\diamond}_{\text{hot}} = 1750\,\text{kW/m}^2$$
$$h^{\diamond}_{\text{water}} = 45\,\text{kW/(m}^2\cdot\text{K)}$$
$$\bar{T}^{\diamond}_{\text{water}} = 25\,^{\circ}\text{C}$$

$$T_{\text{3D,hot}} = 192.6\,^{\circ}\text{C}$$
$$T_{\text{3D,TC}} = 103.8\,^{\circ}\text{C}$$

Channel	A_c mm^2	$D_{h,c}$ mm	$T_{c,avg}$ °C	$T_{c,max}$ °C
1	105.0	8.077	44.78	72.54
2	90.0	7.826	37.93	59.84
3	90.0	7.826	38.33	60.37
4	90.0	7.826	38.35	60.40
5	90.0	7.826	37.72	60.43
Total	420.0			
ROM	93.33	7.882	39.42	72.54

Model	w_c mm	d_c mm	p_c mm	d_{plate} mm	$d_{c,max}$ mm	$d_{c,avg}$ mm	d_{TC} mm
Uncalibrated ROM	5.0	18.0	15.0	27.0			22.0
Calibrated ROM	4.994	18.69	17.22	27.51	24.98	31.87	18.48

Fig. 7. Calibration domain geometry, conditions, and results for Mould B [29].

The conditions for insensitivity of d_{plate} to the other calibration parameters are

$$\left|\frac{\partial d_{\text{plate}}}{\partial k_{\text{mould}}}\right| \ll \frac{d_{\text{plate}}}{k_{\text{mould}}}, \tag{41}$$

$$\left|\frac{\partial d_{\text{plate}}}{\partial h_{\text{water}}}\right| \ll \frac{k_{\text{mould}}}{h^2_{\text{cold}}}\left(\left(\frac{w_c}{p_c}\right)+\left(1-\frac{w_c}{p_c}\right)\left(\frac{\tanh(\beta)+\beta\left(1-\tanh^2(\beta)\right)}{2\sqrt{(p_c-w_c)h_{\text{water}}/(2k_{\text{mould}})}}\right)\right), \tag{42}$$

$$\left|\frac{\partial d_{\text{plate}}}{\partial \bar{T}_{\text{water}}}\right| \ll \frac{k_{\text{mould}}}{q_{\text{hot}}}. \tag{43}$$

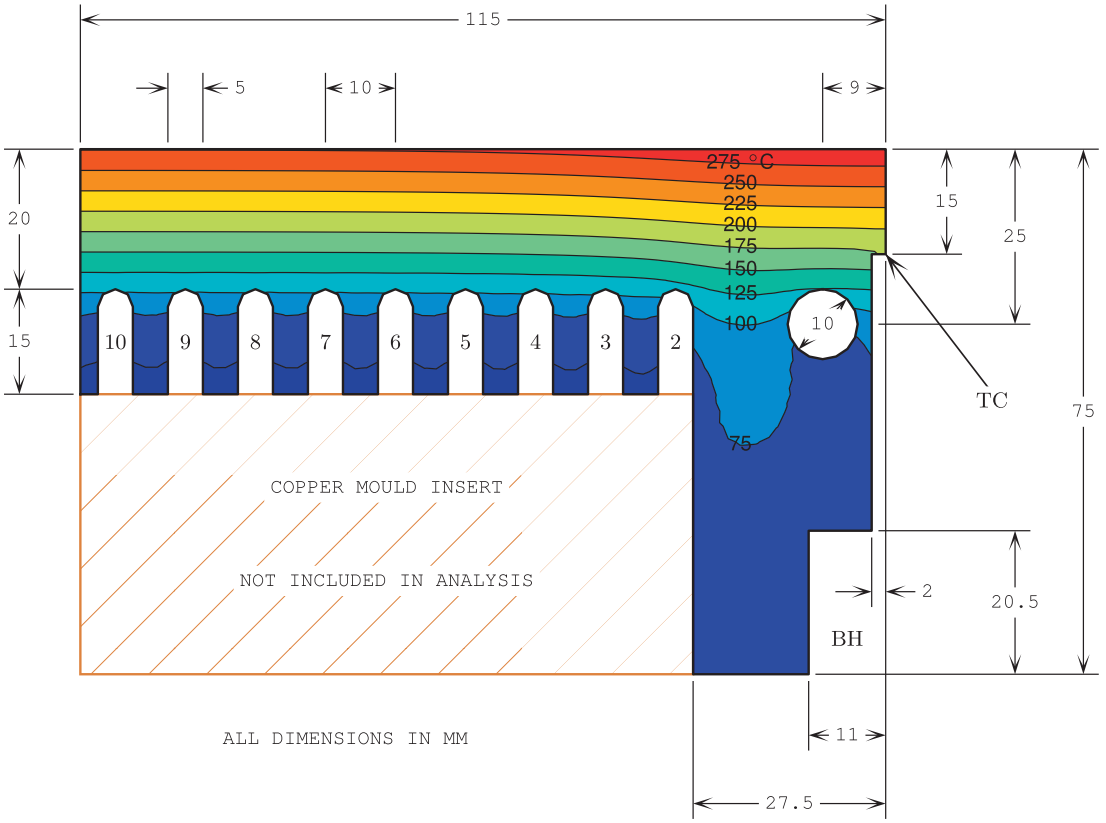

$$k^{\diamond}_{\text{mould}} = 350\,\text{W/(m}\cdot\text{K)}$$
$$q^{\diamond}_{\text{hot}} = 3000\,\text{kW/m}^2$$
$$h^{\diamond}_{\text{water}} = 36\,\text{kW/(m}^2\cdot\text{K)}$$
$$\bar{T}^{\diamond}_{\text{water}} = 40\,^{\circ}\text{C}$$

$$T_{\text{3D,hot}} = 282.5\,^{\circ}\text{C}$$
$$T_{\text{3D,TC}} = 179.6\,^{\circ}\text{C}$$

Channel	A_c mm^2	$D_{h,c}$ mm	$T_{c,avg}$ °C	$T_{c,max}$ °C
1	78.54	10.0	91.18	124.1
2	72.32	7.642	72.04	115.9
3	72.32	7.642	63.58	109.3
4	72.32	7.642	62.85	107.4
5	72.32	7.642	62.52	106.4
6	72.32	7.642	62.37	105.9
7	72.32	7.642	62.24	105.5
8	72.32	7.642	62.20	105.5
9	72.32	7.642	62.16	105.4
10	72.32	7.642	62.17	105.3
Total	729.4			
ROM	72.94	7.878	66.33	124.1

Model	w_c mm	d_c mm	p_c mm	d_{plate} mm	$d_{c,max}$ mm	$d_{c,avg}$ mm	d_{TC} mm
Uncalibrated ROM	5.0	14.0	10.0	21.0			15.0
Calibrated ROM	5.682	12.84	11.50	21.37	18.47	25.22	12.01

Fig. 8. Calibration domain geometry, conditions, and results for Mould c [36].

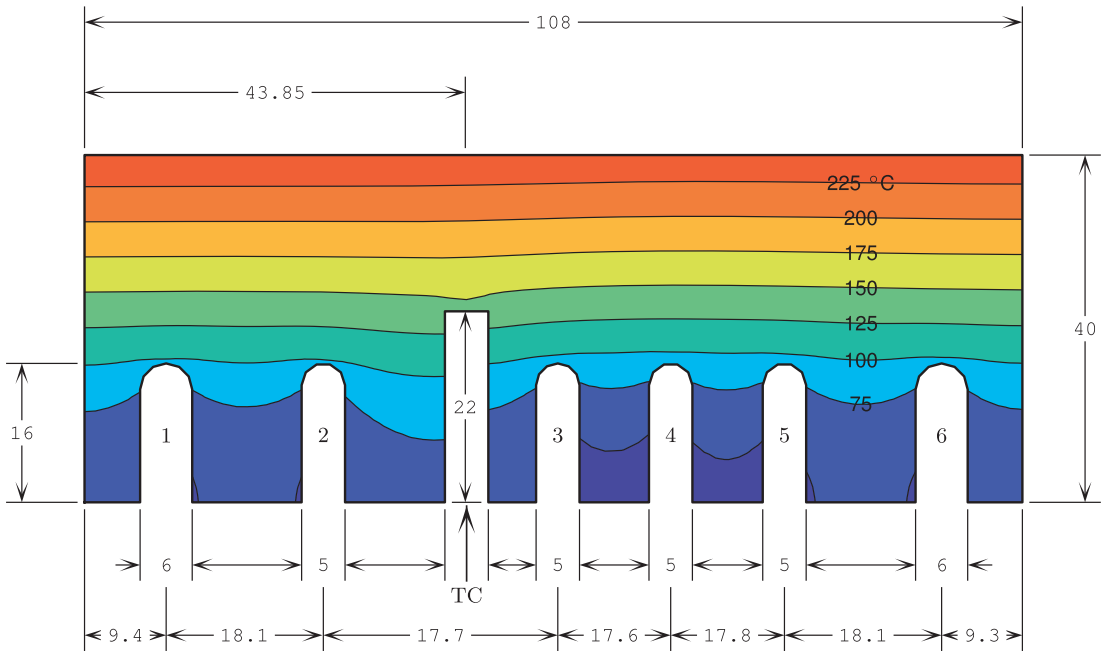

ALL DIMENSIONS IN MM WATER CHANNEL PITCHES REFLECT GEOMETRY AWAY FROM THERMOCOUPLE HOLE

$$k^{\diamond}_{\text{mould}} = 340\,\text{W/(m}\cdot\text{K)}$$
$$q^{\diamond}_{\text{hot}} = 2100\,\text{kW/m}^2$$
$$h^{\diamond}_{\text{water}} = 32.5\,\text{kW/(m}^2\cdot\text{K)}$$
$$\bar{T}^{\diamond}_{\text{water}} = 31\,^{\circ}\text{C}$$

$$T_{\text{3D,hot}} = 245.7\,^{\circ}\text{C}$$
$$T_{\text{3D,TC}} = 146.7\,^{\circ}\text{C}$$

Channel	A_c mm^2	$D_{h,c}$ mm	$T_{c,avg}$ °C	$T_{c,max}$ °C
1	92.14	8.897	60.64	96.65
2	77.32	7.760	62.39	96.76
3	77.32	7.760	57.95	93.57
4	77.32	7.760	55.34	90.69
5	77.32	7.760	57.53	92.35
6	92.14	8.897	60.02	95.47
Total	493.5			
ROM	82.26	8.139	58.98	96.76

Model	w_c mm	d_c mm	p_c mm	d_{plate} mm	$d_{c,max}$ mm	$d_{c,avg}$ mm	d_{TC} mm
Uncalibrated ROM	5.333	15.0	18.4	25.0			18.0
Calibrated ROM	5.647	14.57	18.0	25.75	24.12	30.24	16.03

Fig. 9. Calibration domain geometry, conditions, and results for Mould D [27].

The sensitivity criteria of Eqs. (40)–(43) are explored here for Mould A; the other moulds in Section 5 produce similar results. The calibration procedure was performed many times over a wide range of values of the non-geometric parameters $q^{\diamond}_{\text{hot}}$, $k^{\diamond}_{\text{mould}}$, $h^{\diamond}_{\text{water}}$, and $\bar{T}^{\diamond}_{\text{water}}$ to create smooth approximations to the derivatives. Fig. 10 shows the right sides of Eqs. (40)–(43) as solid lines and the approximate derivatives from the numerical study as × 's. The value of d_{plate} is:

- independent of the heat load $q^{\diamond}_{\text{hot}}$: the derivative with respect to $q^{\diamond}_{\text{hot}}$ is less than 10^{-9}m^3/MW, which is much smaller than the limit predicted by Eq. (40) and likely is round-off error,
- weakly sensitive to the mould thermal conductivity $k^{\diamond}_{\text{mould}}$: the maximum derivative with respect to $k^{\diamond}_{\text{mould}}$ is 2.5 × 10^{-3}m^2 · K/kW, which is 5% or less of the limit predicted by Eq. (41), and

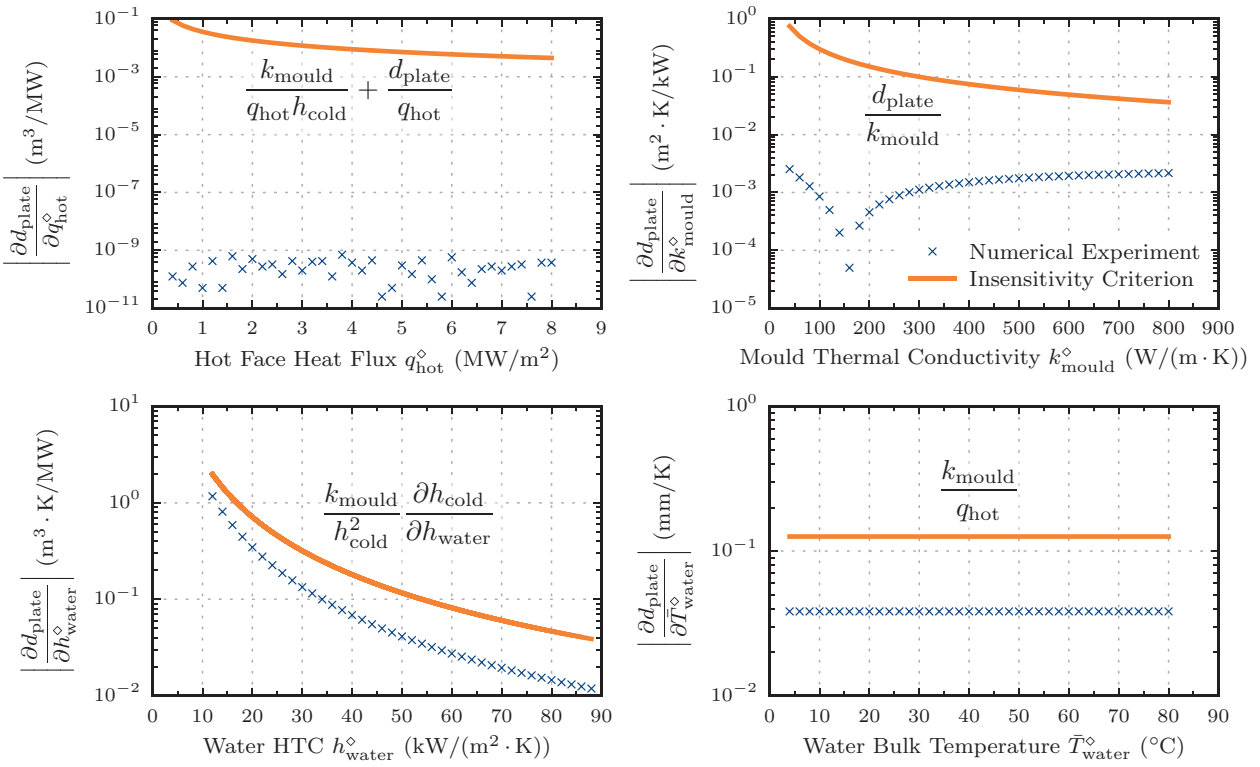

Fig. 10. Sensitivity of the calibrated mould plate thickness to non-geometric ROM parameters.

- somewhat sensitive to the water HTC $h^{\diamond}_{\text{water}}$ and bulk temperature $\bar{T}^{\diamond}_{\text{water}}$: the derivatives with respect to these variables are about 30% of the limits predicted by Eqs. (42) and (43).

In practice, the accuracy is better than these results suggest: calibrating the ROM with $h^{\diamond}_{\text{water}} = 40$ kW/(m²K) and then using it with $h_{\text{water}} = 50$ kW/(m²K) corresponds to an error of about 0.6 mm in d_{plate}, which causes about 4 °C error in the calculated mould temperatures. Across a typical continuous casting mould, the value of h_{water} deviates by about 5% from its average, and the value of $\bar{T}_{\text{water}}$ changes by about 10 °C, so the sensitivity to these parameters is tolerable. The insensitivity to the heat load q_{hot} is perhaps the most crucial aspect of this ROM because the value of q_{hot} varies widely and is the least well-known of all the boundary conditions on the mould. As long as reasonable average values of h_{water} and $\bar{T}_{\text{water}}$ are used in the calibration, the ROM robustly produces the relationship between the input heat flux and output mould temperatures, and is an efficient and accurate modelling tool.

7. Applications of the reduced-order model

The fast and accurate ROM developed in this work has been applied as part of a comprehensive model of solidification heat transfer during continuous casting of steel [19,64]. In addition, the 1D temperature solution presented in Section 2.1 also has other practical applications as part of coupled, higher-order models of the continuous casting process.

7.1. Implementing the ROM into 2D and 3D heat transfer calculations

To incorporate the ROM into a finite-element or finite-volume model, the mould is modelled as a single layer of elements or cells with a convection condition applied on the "cold" side of the layer with $\bar{T}_{\text{water}}$ as the sink temperature. One variant of this modelling technique has the temperatures of the hot and cold sides of the layer constrained to be equal, so the layer thickness is arbitrary, and the cold-side HTC is

$$\frac{1}{h_{\text{mould}}} = \frac{1}{h_{\text{cold}}} + \frac{d_{\text{plate}}}{k_{\text{mould}}} + \frac{d_{\text{coat}}}{k_{\text{coat}}}. \tag{44}$$

All geometric parameters are calibrated as described in Section 4. Other 1D model approximations of mould heat transfer [19,29,34,64] produce similar forms of this effective HTC, but do not meet the accuracy of the ROM presented in this work. In a particular implementation with the ABAQUS user subroutine FILM, the estimated hot face temperature T_{hot} is

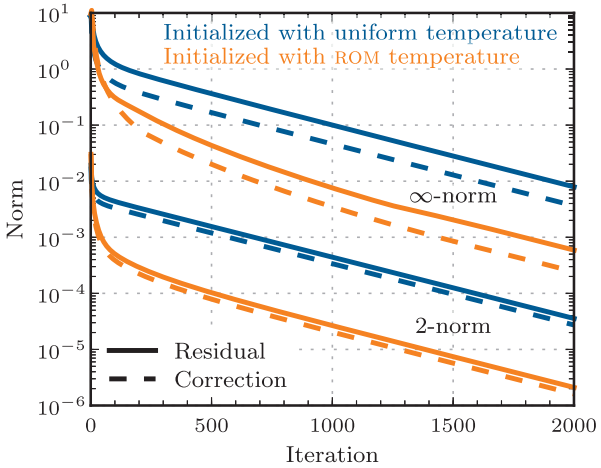

Fig. 11. Behaviour of iterative solution with domain initialised to uniform and ROM-predicted temperature field.

provided as input and h_{mould}, $\partial h_{\text{mould}}/\partial T_{\text{hot}}$, and $\bar{T}_{\text{water}}$ are output back to ABAQUS for global Newton iterations of the finite-element equations. This subroutine, called at every integration point on the surface, performs local Newton iterations on the pair of equations

$$T_{\text{hot}} = \bar{T}_{\text{water}} + q_{\text{hot}}\left(\frac{1}{h_{\text{cold}}(T_{\text{c,avg}})} + \frac{d_{\text{plate}}}{k_{\text{mould}}} + \frac{d_{\text{coat}}}{k_{\text{coat}}}\right) \tag{45}$$

$$T_{\text{c,avg}} = \bar{T}_{\text{water}} + q_{\text{hot}}\left(\frac{1}{h_{\text{cold}}(T_{\text{c,avg}})} + \frac{d_{\text{plate}} + d_{\text{coat}} - d_{\text{c,avg}}}{k_{\text{mould}}}\right) \tag{46}$$

for the local heat flux q_{hot} and the average channel temperature $T_{\text{c,avg}}$. If h_{water} is independent of temperature then the iterations are not necessary. Reasonable initial values for the iterations are attained by assuming $\text{Nu} = 300$ and solving for q_{hot} and $T_{\text{c,avg}}$. The mould HTC then is

$$h_{\text{mould}} = \frac{q_{\text{hot}}}{T_{\text{hot}} - \bar{T}_{\text{water}}}. \tag{47}$$

A variant of this approach has been applied with success in previous work [22,23].

An alternative method to implement the ROM allows heat conduction in the y- and z-directions. The ROM presented in Section 2 loses accuracy in the region of initial solidification because the cold region above the liquid level and the large axial gradient of mould heat flux below the liquid level both drive additional heat flow perpendicular to the direction modelled by the ROM. A solution to this issue is to model the mould as a simple quadrilateral (in 2D) or hexahedral (in 3D) domain, with thickness equal to the calibrated value of d_{plate} from Eq. (33), and a convection condition on the cold side with HTC of h_{cold} as described in Section 2.2 and sink temperature of $\bar{T}_{\text{water}}$. This implementation of the ROM captures some of the axial and transverse conduction effects, such as near the meniscus and slab corners, that are not captured in the 1D temperature solution on which the ROM is based. Steady-state simulations need only one finite element in the thickness direction, and transient simulations require a few layers. Though inconsistent with some of the assumptions in the 1D solution, such as the fin equation being valid only for steady-state conditions, the inaccuracies in this approach are expected to be small.

7.2. Initial value for iterative solutions of mould heat transfer

Another use of the ROM is to provide intelligent initial values of the temperature field for iterative solutions of the steady-state heat transfer in two- or three-dimensional analyses of the mould. To demonstrate this technique, consider a longitudinal (x–z) plane of Mould C in Section 5, modelled as a rectangle, with a calibrated [36] heat flux profile $q_{\text{hot}}(z)$ supplied on the hot face, a convection condition with h_{cold} from Eq. (6) applied on the cold face, and the top and bottom faces insulated. The steady heat-conduction equation is discretised with the finite-difference method for 22 grid points through the thickness of the mould and 551 grid points along the length of the mould for approximately 2 mm spacing, and the resulting equations are solved with Gauss–Seidel iterations [74]. The mould plate thickness d_{plate} is calculated with Eq. (33). The domain is initialised either uniformly at the water temperature, or using the ROM temperature solution given in Eq. (2) in lines of constant z across the domain. Fig. 11 shows the unscaled ∞- and 2-norms of the temperature residual and correction vectors the for the first 2000 iterations for these two initialisation approaches. The first 200 iterations of the

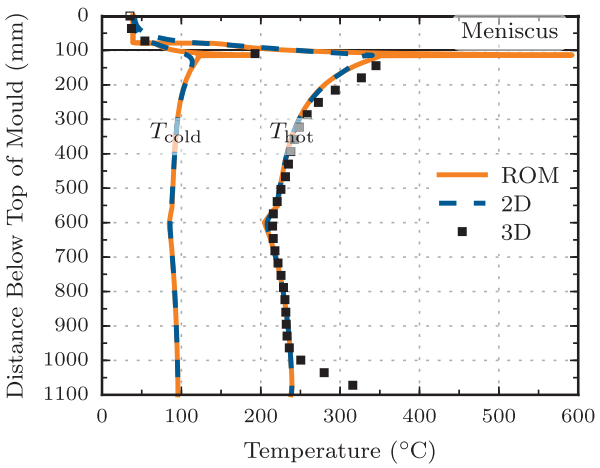

Fig. 12. Comparison of hot and cold face temperatures from ROM and iterative 2D solutions.

ROM-initialised solution shows a much more rapid convergence rate than the uniformly-initialised solution, which indicates that the ROM carries the dominant, lower-frequency components of the solution. The residual norms for the ROM-initialised solution usually are about one order of magnitude lower than the uniformly-initialised solution.

To further demonstrate the technique, the predictions of the ROM are compared with a 3D finite-element analysis of the mould [26]. The 3D mesh has 855,235 elements and 4,223,072 nodes and the complete mould geometry, including the funnel, the curved water channel roots, and the thermocouple holes. The water channel surfaces have a convection condition with h_{water} from Eq. (12), and the same calibrated heat flux profile described above applied on the hot face.

Fig. 12 compares the temperature predictions of the ROM, the converged 2D iterative solution, and the 3D finite-element solution. Except for within about 50 mm of the meniscus, the ROM solution matches closely with both the 2D and 3D solutions for the hot face temperature and the nominal cold face temperature profiles. As mentioned earlier, the cold region above the liquid level increases the importance of the axial heat conduction near the meniscus. The hot face temperature in the 3D model increases near the bottom of the mould because of the changing geometry of the water channels, which is not captured with the lower-order models. The heat diffusion is more pronounced near the meniscus in the 3D model than in the lower-order models for the reasons previously discussed, resulting in the peak temperature occurring slightly further down the mould. The close agreement observed over most of the mould length provides additional evidence that the ROM calibration procedure is independent of the particular choice of calibration parameters.

For the same mesh density, calculating the 2D temperature field with the ROM requires about 10% or less of the time required for a single Gauss–Seidel iteration of the 2D solution, and can save many hundreds of iterations. For example, converging to e-3 requires about 218 s with the uniform-initialised 2D model but only 13 s with the ROM-initialised 2D model. The 3D model requires weeks to create the geometry and mesh, and about 15 min for the analysis. The ROM execution time of milliseconds has marked advantage over the higher-order models, especially when used as part of coupled process models.

8. Conclusions

A reduced-order model (ROM) has been developed by calibrating some of the geometric parameters in a simple analytical solution that contains most of the physics of the problem. The methodology has been demonstrated specifically for mould heat transfer in the continuous casting of steel, and a rigorous procedure for calibrating the geometric parameters for the mould is presented. The “blueprint” values of the mould geometry are changed by about 10% in the ROM to compensate for multi-dimensional heat transfer. This approach was demonstrated to be independent of the calibration values of heat flux and mould thermal conductivity, and slightly sensitive to the calibration values of water channel heat transfer coefficient and bulk temperature. Using appropriate values for these two parameters during calibration allows the ROM calibration procedure to be performed only once per mould geometry. The calibrated ROM enables other more comprehensive models of continuous casting process phenomena to include accurate mould heat transfer with negligible additional computational cost.

Acknowledgements

The financial support of the member companies of the Continuous Casting Consortium at the University of Illinois at Urbana-Champaign is acknowledged gratefully. At the time of writing, the members are: ABB, ArcelorMittal, Baosteel, Magnesita Refractories, Nippon Steel & Sumitomo Metal Corp., Nucor Steel Decatur, POSTECH/POSCO, Severstal, SSAB,

Tata Steel, and ANSYS-FLUENT. Inwho Hwang is acknowledged for his assistance in developing some computational tools for early versions of this work.

References

[1] L.T. Pillage, R.A. Rohrer, Asymptotic waveform evaluation for timing analysis, IEEE Trans. Comput. Aided Des. Integr. Circuits Syst. 9 (4) (1990) 352–366, doi:10.1109/43.45867.

[2] P. Feldmann, R.W. Freund, Efficient linear circuit analysis by Padé approximation via the Lanczos process, IEEE Trans. Comput. Aided Des. Integr. Circuits Syst. 14 (5) (1995) 639–649, doi:10.1109/43.384428.

[3] D. González, E. Cueto, F. Chinesta, Real-time direct integration of reduced solid dynamics equations, Int. J. Numer. Methods Eng. (2014), doi:10.1002/nme.4691. in press

[4] G. Kerschen, J.-C. Golinval, A.F. Vakakis, L.A. Bergman, The method of proper orthogonal decomposition for dynamical characterization and order reduction of mechanical systems: an overview, Nonlinear Dyn. 41 (1–3) (2005) 147–169, doi:10.1007/s11071-005-2803-2.

[5] L.S. Louca, Modal analysis reduction of multi-body systems with generic damping, J. Comput. Sci. 5 (3) (2014) 415–426, doi:10.1016/j.jocs.2013.08.008.

[6] A. Lozovskiy, The modal reduction method for multi-body dynamics with non-smooth contact, Int. J. Numer. Methods Eng. 98 (13) (2014) 937–959, doi:10.1002/nme.4651.

[7] J. Barbič, D.L. James, Real-time subspace integration for St. Venant–Kirchhoff deformable models, ACM Trans. Graph. 24 (3) (2005) 982–990, doi:10.1145/1073204.1073300.

[8] J. Burkardt, M. Gunzburger, H.-C. Lee, POD and CVT-based reduced-order modeling of Navier–Stokes flows, Comput. Methods Appl. Mech. Eng. 196 (1–3) (2006) 337–355, doi:10.1016/j.cma.2006.04.004.

[9] D. Alonso, A. Velazquez, J.M. Vega, Robust reduced order modeling of heat transfer in a back step flow, Int. J. Heat Mass Transf. 52 (5–6) (2009) 1149–1157, doi:10.1016/j.ijheatmasstransfer.2008.09.011.

[10] Y. Favennec, Y. Rouizi, D. Petit, On the use of reduced models obtained through identification for feedback optimal control problems in a heat convection-diffusion problem, Comput. Methods Appl. Mech. Eng. 199 (17–20) (2010) 1193–1201, doi:10.1016/j.cma.2009.12.009.

[11] Y. Rouizi, Y. Favennec, J. Ventura, D. Petit, Numerical model reduction of 2D steady incompressible laminar flows: application on the flow over a backward-facing step, J. Comput. Phys. 228 (6) (2009) 2239–2255, doi:10.1016/j.jcp.2008.12.001.

[12] D. Amsallem, M.J. Zahr, C. Farhat, Nonlinear model order reduction based on local reduced-order bases, Int. J. Numer. Methods Eng. 92 (10) (2012) 891–916, doi:10.1002/nme.4371.

[13] T. Lieu, C. Farhat, M. Lesoinne, Reduced-order fluid/structure modeling of a complete aircraft configuration, Comput. Methods Appl. Mech. Eng. 195 (41–43) (2006) 5730–5742, doi:10.1016/j.cma.2005.08.026.

[14] S. Walton, O. Hassan, K. Morgan, Reduced order modelling for unsteady fluid flow using proper orthogonal decomposition and radial basis functions, Appl. Math. Model. 37 (20–21) (2013) 8930–8945, doi:10.1016/j.apm.2013.04.025.

[15] W.Q. Wang, Y. Yan, Strongly coupling of partitioned fluid-solid interaction solvers using reduced-order models, Appl. Math. Model. 34 (12) (2010) 3817–3830, doi:10.1016/j.apm.2010.03.022.

[16] G. Berkooz, P. Holmes, J.L. Lumley, The proper orthogonal decomposition in the analysis of turbulent flows, Annu. Rev. Fluid Mech. 25 (1993) 539–575, doi:10.1146/annurev.fl.25.010193.002543.

[17] P. Pacciarini, G. Rozza, Stabilized reduced basis method for parametrized advection-diffusion PDEs, Comput. Methods Appl. Mech. Eng. 274 (2014) 1–18, doi:10.1016/j.cma.2014.02.005.

[18] D.J. Lucia, P.S. Beran, W.A. Silva, Reduced-order modeling: new approaches for computational physics, Prog. Aerosp. Sci. 40 (1–2) (2004) 51–117, doi:10.1016/j.paerosci.2003.12.001.

[19] B. Ho, Characterization of Interfacial Heat Transfer in the Continuous Slab Casting Process, The University of Illinois at Urbana-Champaign, 1991 (Master's thesis).

[20] Y. Meng, B.G. Thomas, Modeling transient slag-layer phenomena in the shell/mold gap in continuous casting of steel, Metall. Mater. Trans. B 34 (5) (2003) 707–725, doi:10.1007/s11663-003-0041-x.

[21] Y. Meng, B.G. Thomas, Simulation of microstructure and behavior of interfacial mold slag layers in continuous casting of steel, ISIJ Int. 46 (5) (2006) 660–669, doi:10.2355/isijinternational.46.660.

[22] L.C. Hibbeler, K. Xu, B.G. Thomas, S. Koric, C. Spangler, Thermomechanical modeling of beam blank casting, Iron Steel Technol. 6 (7) (2009) 60–73.

[23] S. Koric, L.C. Hibbeler, R. Liu, B.G. Thomas, Multiphysics model of metal solidification on the continuum level, Num. Heat Transf. B 58 (6) (2010) 371–392, doi:10.1080/10407790.2011.540954.

[24] J.-E. Lee, T.-J. Yeo, K.H. Oh, J.-K. Yoon, U.-S. Yoon, Prediction of cracks in continuously cast steel beam blank through fully coupled analysis of fluid flow, heat transfer, and deformation behavior of a solidifying shell, Metall. Mater. Trans. A 31 (1) (2000) 225–237, doi:10.1007/s11661-000-0067-5.

[25] H.L. Xu, G.H. Wen, W. Sun, K.Z. Wang, B. Yan, W. Luo, Thermal behaviour of moulds with different water channels and their influence on quality in continuous casting of beam blanks, Ironmak. Steelmak. 37 (5) (2010) 380–386, doi:10.1179/030192310X12646889255780.

[26] L.C. Hibbeler, B.G. Thomas, R.C. Schimmel, G. Abbel, The thermal distortion of a funnel mold, Metall. Mater. Trans. B 43 (5) (2012) 1156–1172, doi:10.1007/s11663-012-9696-5.

[27] L.C. Hibbeler, M.M. Langeneckert, J. Iwasaki, I. Hwang, B.G. Thomas, R.J. O'Malley, Calibration of thermal models of steel continuous casting molds, Iron Steel Technol. 10 (9) (2013) 199–210.

[28] E.-Y. Ko, K.-W. Yi, J.-K. Park, J.W. Cho, H.-J. Shin, Numerical modeling and analysis of the thermal behavior of copper molds in continuous casting, Met. Mater. Int. 16 (2) (2010) 281–288, doi:10.1007/s12540-010-0418-8.

[29] M.M. Langeneckert, Influence of Mold Geometry on Heat Transfer, Thermocouple and Mold Temperatures in the Continuous Casting of Steel Slabs, The University of Illinois at Urbana-Champaign, 2001 (Master's thesis).

[30] B.G. Thomas, M. Langeneckert, L. Castellá, M. Dziuba, G. di Gresia, W. Balante, Optimisation of narrow face water slot design for Siderar slab casting mould, Ironmak. Steelmak. 30 (3) (2003) 235–239, doi:10.1179/030192303225009579.

[31] X. Xie, D. Chen, H. Long, M. Long, K. Lv, Mathematical modeling of heat transfer in mold copper coupled with cooling water during the slab continuous casting process, Metall. Mater. Trans. B (2014), doi:10.1007/s11663-014-0127-7.

[32] J.E. Camporredondo, A.H. Castillejos, F.A. Acosta, E.P. Gutiérrez, M.A. Herrera, Analysis of thin-slab casting by the compact-strip process: part I. Heat extraction and solidification, Metall. Mater. Trans. B 35 (3) (2004) 541–560, doi:10.1007/s11663-004-0054-0.

[33] X. Meng, M. Zhu, Thermal behavior of hot copper plates for slab continuous casting mold with high casting speed, ISIJ Int. 49 (9) (2009) 1356–1361, doi:10.2355/isijinternational.49.1356.

[34] U. Ölmann, K. Schwerdtfeger, Heat transfer through the copper plate of slab moulds, Steel Res. Int. 77 (3) (2006) 186–193.

[35] I.V. Samarasekera, J.K. Brimacombe, The thermal field in continuous-casting moulds, Can. Metall. Q. 18 (3) (1979) 251–266, doi:10.1179/000844379795317670.

[36] B. Santillana, L.C. Hibbeler, B.G. Thomas, A. Hamoen, A. Kamperman, W. van der Knoop, Heat transfer in funnel-mould casting: effect of plate thickness, ISIJ Int. 48 (10) (2008) 1380–1388, doi:10.2355/isijinternational.48.1380.

[37] I.V. Samarasekera, D.L. Anderson, J.K. Brimacombe, The thermal distortion of continuous-casting billet molds, Metall. Trans. B 13 (1) (1982) 91–104, doi:10.1007/BF02666960.

[38] I.V. Samarasekera, J.K. Brimacombe, The influence of mold behavior on the production of continuously cast steel billets, Metall. Trans. B 13 (1) (1982) 105–116, doi:10.1007/BF02666961.

[39] Y.-M. Xie, S.-R. Yin, Three-dimensional thermal stress analysis of the mould during high-speed casting of steel, J. Strain Anal. Eng. Des. 43 (7) (2008) 565–568, doi:10.1243/03093247JSA435.
[40] H. Yin, M. Yao, H. Zhan, D. Fang, 3D stress model with friction in and of mould for round billet continuous casting, ISIJ Int. 46 (4) (2006) 546–552, doi:10.2355/isijinternational.46.546.
[41] J. Zhou, X. Peng, Y. Qin, A coupled thermal-mechanical analysis of a mold-billet system during continuous casting, Int. J. Adv. Manuf. Technol. 42 (5–6) (2009) 421–428, doi:10.1007/s00170-008-1620-4.
[42] X. Liu, M. Zhu, Finite element analysis of thermal and mechanical behavior in a slab continuous casting mold, ISIJ Int. 46 (11) (2006) 1652–1659, doi:10.2355/isijinternational.46.1652.
[43] X. Peng, J. Zhou, Y. Qin, Improvement of the temperature distribution in continuous casting moulds through the rearrangement of the cooling water slots, J. Mater. Process. Technol. 167 (2–3) (2005) 508–514, doi:10.1016/j.jmatprotec.2005.05.023.
[44] B.G. Thomas, G. Li, A. Moitra, D. Habing, Analysis of thermal and mechanical behavior of copper molds during continuous casting of steel slabs, Iron Steelmak. 25 (10) (1998) 125–143.
[45] J.K. Park, I.V. Samarasekera, B.G. Thomas, U.S. Yoon, Thermal and mechanical behavior of copper molds during thin-slab casting (I): plant trial and mathematical modeling, Metall. Mater. Trans. B 33 (3) (2002a) 425–436, doi:10.1007/s11663-002-0054-x.
[46] J.K. Park, I.V. Samarasekera, B.G. Thomas, U.S. Yoon, Thermal and mechanical behavior of copper molds during thin-slab casting (II): mold crack formation, Metall. Mater. Trans. B 33 (3) (2002b) 437–449, doi:10.1007/s11663-002-0055-9.
[47] V.K. de Barcellos, C.R.F. Ferreira, C.A. dos Santos, J.A. Spim, Analysis of metal mould heat transfer coefficients during continuous casting of steel, Ironmak. Steelmak. 37 (1) (2010) 47–56, doi:10.1179/030192309X12506804200942.
[48] C. Chow, I.V. Samarasekera, B.N. Walker, G. Lockhart, High speed continuous casting of steel billets: part 2: mould heat transfer and mould design, Ironmak. Steelmak. 29 (1) (2002) 61–69, doi:10.1179/030192302225001947.
[49] C.A.M. Pinheiro, I.V. Samarasekera, J.K. Brimacombe, B.N. Walker, Mould heat transfer and continuously cast billet quality with mould flux lubrication: part 1: mould heat transfer, Ironmak. Steelmak. 27 (1) (2000) 37–54, doi:10.1179/030192300677363.
[50] Y. Xie, H. Yu, X. Ruan, B. Wang, Y. Ma, FE numerical simulation of mould temperature field during the continuous casting of steel, Int. J. Adv. Manuf. Technol. 30 (7–8) (2006) 645–651, doi:10.1007/s00170-005-0100-3.
[51] M. Yao, H. Yin, D. Fang, Real-time analysis on non-uniform heat transfer and solidification in mould of continuous casting round billets, ISIJ Int. 44 (10) (2004) 1696–1704, doi:10.2355/isijinternational.44.1696.
[52] H. Yin, M. Yao, D. Fang, 3-D inverse problem continuous model for thermal behavior of mould process based on the temperature measurements in plant trial, ISIJ Int. 46 (4) (2006) 539–545, doi:10.2355/isijinternational.46.539.
[53] R. Chen, H.F. Shen, B.C. Liu, Numerical simulation of fluid flow and solidification in continuous slab casting mould based on inverse heat transfer calculation, Ironmak. Steelmak. 38 (7) (2011) 546–551, doi:10.1179/1743281211Y.0000000049.
[54] R.B. Mahapatra, J.K. Brimacombe, I.V. Samarasekera, N. Walker, E.A. Paterson, J.D. Young, Mold behavior and its influence on quality in the continuous casting of steel slabs: part I. Industrial trials, mold temperature measurements, and mathematical modeling, Metall. Trans. B 22 (6) (1991) 861–874, doi:10.1007/BF02651163.
[55] X. Wang, L. Tang, X. Zang, M. Yao, Mold transient heat transfer behavior based on measurement and inverse analysis of slab continuous casting, J. Mater. Process. Technol. 212 (9) (2012) 1811–1818, doi:10.1016/j.jmatprotec.2012.04.001.
[56] H.N. Han, J.-E. Lee, T.-J. Yeo, Y.M. Won, K.-H. Kim, K.H. Oh, J.-K. Yoon, A finite element model for 2-dimensional slice of cast strand, ISIJ Int. 39 (5) (1999) 445–454, doi:10.2355/isijinternational.39.445.
[57] D. Zhang, S. Lei, S. Zeng, H. Shen, Thermo-mechanical modeling in continuous slab casting mould and its application, ISIJ Int. 54 (2) (2014) 336–341, doi:10.2355/isijinternational.54.336.
[58] H. Nam, H.-S. Park, J.K. Yoon, Numerical analysis of fluid flow and heat transfer in the funnel type mold of a thin slab caster, ISIJ Int. 40 (9) (2000) 886–892, doi:10.2355/isijinternational.40.886.
[59] H.-S. Park, H. Nam, J.K. Yoon, Numerical analysis of fluid flow and heat transfer in the parallel type mold of a thin slab caster, ISIJ Int. 41 (9) (2001) 974–980, doi:10.2355/isijinternational.41.974.
[60] P.E. Ramirez-Lopez, U. Sjöström, P.D. Lee, K.C. Mills, B. Jonsson, J. Janis, A novel approach for coupling slag infiltration to metal flow, solidification and mold oscillation on 3D model for continuous casting of slabs, in: Proc. AISTech, 2012, pp. 1259–1268.
[61] J.E. Kelly, K.P. Michalek, T.G. O'Connor, B.G. Thomas, J.A. Dantzig, Initial development of thermal and stress fields in continuously cast steel billets, Metall. Trans. A 19 (10) (1988) 2589–2602, doi:10.1007/BF02645486.
[62] J.-E. Lee, H.N. Han, K.H. Oh, J.-K. Yoon, A fully coupled analysis of fluid flow, heat transfer and stress in continuous round billet casting, ISIJ Int. 39 (5) (1999) 435–444, doi:10.2355/isijinternational.39.435.
[63] T.G. O'Connor, J.A. Dantzig, Modeling the thin-slab continuous-casting mold, Metall. Mater. Trans. B 25 (3) (1994) 443–457, doi:10.1007/BF02663395.
[64] Y. Meng, B.G. Thomas, Heat-transfer and solidification model of continuous slab casting: CON1D, Metall. Mater. Trans. B 34 (5) (2003) 685–705, doi:10.1007/s11663-003-0040-y.
[65] M.R. Ridolfi, B.G. Thomas, G. Li, U.D. Foglia, The optimization of mold taper for the Ilva–Dalmine round bloom caster, Rev. Métall. 91 (4) (1994) 609–620.
[66] J. Sengupta, M.K. Trinh, D. Currey, B.G. Thomas, Utilization of CON1D at ArcelorMittal Dofasco's no. 2 continuous caster for crater end determination, in: Proc. AISTech, 2009, pp. 1177–1185.
[67] J.A. Dantzig, C.L. Tucker, Modeling in Materials Processing, Cambridge University Press, 2001, doi:10.1017/CBO9781139175272.
[68] H. Gilles, Primary and Secondary Cooling Control, vol. 5, 11th ed., AISE Steel Foundation, 2003. chap. 5
[69] A.D. Kraus, A. Aziz, J. Welty, Extended Surface Heat Transfer, John Wiley & Sons, Inc., 2007, doi:10.1002/9780470172582.
[70] C.A. Sleicher, M.W. Rouse, A convenient correlation for heat transfer to constant and variable property fluids in turbulent pipe flow, Int. J. Heat Mass Transf. 18 (5) (1975) 677–683, doi:10.1016/0017-9310(75)90279-3.
[71] D.R. Lide (Ed.), CRC Handbook of Chemistry and Physics, 78th ed., 1997, p. 3. chap. 6
[72] NIST Chemistry WebBook, 2011.
[73] ABAQUS, ABAQUS 6.13 User Manuals, Dassault Simulia, 2013.
[74] R.H. Pletcher, J.C. Tannehill, D. Anderson, Computational Fluid Mechanics and Heat Transfer, third ed., CRC Press, 2012.